NUREG/CR-6894
PNNL-15346

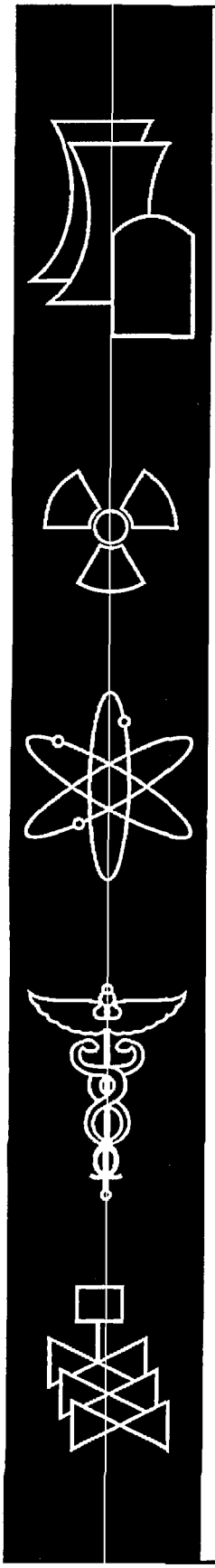

Spent Fuel Transportation Package Response to the Caldecott Tunnel Fire Scenario

Draft Report for Comment

Pacific Northwest National Laboratory

U.S. Nuclear Regulatory Commission
Office of Nuclear Material Safety and Safeguards
Washington, DC 20555-0001

AVAILABILITY OF REFERENCE MATERIALS IN NRC PUBLICATIONS

NRC Reference Material

As of November 1999, you may electronically access NUREG-series publications and other NRC records at NRC's Public Electronic Reading Room at http://www.nrc.gov/reading-rm.html. Publicly released records include, to name a few, NUREG-series publications; *Federal Register* notices; applicant, licensee, and vendor documents and correspondence; NRC correspondence and internal memoranda; bulletins and information notices; inspection and investigative reports; licensee event reports; and Commission papers and their attachments.

NRC publications in the NUREG series, NRC regulations, and *Title 10, Energy*, in the Code of *Federal Regulations* may also be purchased from one of these two sources.

1. The Superintendent of Documents
   U.S. Government Printing Office
   Mail Stop SSOP
   Washington, DC 20402–0001
   Internet: bookstore.gpo.gov
   Telephone: 202-512-1800
   Fax: 202-512-2250
2. The National Technical Information Service
   Springfield, VA 22161–0002
   www.ntis.gov
   1–800–553–6847 or, locally, 703–605–6000

A single copy of each NRC draft report for comment is available free, to the extent of supply, upon written request as follows:

Address: Office of the Chief Information Officer,
Reproduction and Distribution
Services Section
U.S. Nuclear Regulatory Commission
Washington, DC 20555-0001
E-mail: DISTRIBUTION@nrc.gov
Facsimile: 301–415–2289

Some publications in the NUREG series that are posted at NRC's Web site address http://www.nrc.gov/reading-rm/doc-collections/nuregs are updated periodically and may differ from the last printed version. Although references to material found on a Web site bear the date the material was accessed, the material available on the date cited may subsequently be removed from the site.

Non-NRC Reference Material

Documents available from public and special technical libraries include all open literature items, such as books, journal articles, and transactions, *Federal Register* notices, Federal and State legislation, and congressional reports. Such documents as theses, dissertations, foreign reports and translations, and non-NRC conference proceedings may be purchased from their sponsoring organization.

Copies of industry codes and standards used in a substantive manner in the NRC regulatory process are maintained at—

The NRC Technical Library
Two White Flint North
11545 Rockville Pike
Rockville, MD 20852–2738

These standards are available in the library for reference use by the public. Codes and standards are usually copyrighted and may be purchased from the originating organization or, if they are American National Standards, from—

American National Standards Institute
11 West 42nd Street
New York, NY 10036–8002
www.ansi.org
212–642–4900

Legally binding regulatory requirements are stated only in laws; NRC regulations; licenses, including technical specifications; or orders, not in NUREG-series publications. The views expressed in contractor-prepared publications in this series are not necessarily those of the NRC.

The NUREG series comprises (1) technical and administrative reports and books prepared by the staff (NUREG–XXXX) or agency contractors (NUREG/CR–XXXX), (2) proceedings of conferences (NUREG/CP–XXXX), (3) reports resulting from international agreements (NUREG/IA–XXXX), (4) brochures (NUREG/BR–XXXX), and (5) compilations of legal decisions and orders of the Commission and Atomic and Safety Licensing Boards and of Directors' decisions under Section 2.206 of NRC's regulations (NUREG–0750).

NUREG/CR-6894
PNNL-15346

Spent Fuel Transportation Package Response to the Caldecott Tunnel Fire Scenario

Draft Report for Comment

Manuscript Completed: January 2006
Date Published: February 2006

Prepared by
H.E. Adkins, Jr., B.J. Koeppel, J. M. Cuta

Pacific Northwest National Laboratory
Richland, WA 99352

A. Hansen, NRC Project Manager

Prepared for
Spent Fuel Project Office
Office of Nuclear Material Safety and Safeguards
U.S. Nuclear Regulatory Commission
Washington, DC 20555-0001
Job Code J5167

COMMENTS ON DRAFT REPORT

Any interested party may submit comments on this report for consideration by the NRC staff. Comments may be accompanied by additional relevant information or supporting data. Please specify the report number NUREG/CR-6894, draft, in your comments, and send them by May 30, 2006 to the following address:

Chief, Rules Review and Directives Branch
U.S. Nuclear Regulatory Commission
Mail Stop T6-D59
Washington, DC 20555-0001

Electronic comments may be submitted to the NRC by the Internet at AGH@nrc.gov.

For any questions about the material in this report, please contact:

Allen Hansen
OWFN 13 D-13
U.S. Nuclear Regulatory Commission
Washington, DC 20555-0001
Phone: 301-415-1390
E-mail: AGH@nrc.gov
Fax: 301-415-8555

ABSTRACT

On April 7, 1982, a tank truck and trailer carrying 8,800 gallons of gasoline was involved in an accident in the Caldecott Tunnel on State Route 24 near Oakland, California. The tank trailer overturned and subsequently caught fire. Because this event is one of the most severe of the five major highway tunnel fires involving shipments of hazardous material that have occurred world wide since 1949, the United States Nuclear Regulatory Commission (USNRC) selected it for analysis to determine the possible regulatory implications of such events for the transportation of spent nuclear fuel by truck.

The Fire Dynamics Simulator (FDS) code developed and maintained by the National Institute of Standards and Technology (NIST) was used to determine the thermal environment in the Caldecott Tunnel during the fire. The FDS results were used to define boundary conditions for a thermal transient model of a truck transport cask containing spent nuclear fuel. The Nuclear Assurance Corporation (NAC) Legal Weight Truck (LWT) transportation cask was selected for this evaluation, as it represents a typical truck (over-the-road) cask.

Detailed analysis of the response of the transport package to the fire was performed using the ANSYS® computer code. The staff concluded that small transportation casks similar to the NAC LWT cask would probably experience degradation of some seals in this severe accident scenario. The maximum temperatures predicted in the regions of the cask lid and the vent and drain ports exceed the rated service temperature of the tetrafluoro-ethylene (TFE) or Viton® seals, making it possible for a small release to occur due to CRUD that might spall off the surfaces of the fuel rods. However, any release is expected to be very small due to a number of factors. These include (1) the metallic lid seal does not exceed its rated service temperature and therefore can be assumed to remain intact, (2) the tight clearances maintained by the lid closure bolts, (3) the low pressure differential between the cask interior and exterior, (4) the tendency for solid particles to plug small clearance gaps and narrow convoluted flow paths such as the vent and drain ports, and (5) the tendency of CRUD particles to settle or plate out and consequently not be available for release.

USNRC staff evaluated the radiological consequences of the package response to the Caldecott Tunnel fire. The results of this evaluation strongly indicate that neither spent nuclear fuel (SNF) particles nor fission products would be released from a spent fuel shipping cask involved in a severe tunnel fire such as the Caldecott Tunnel fire. The NAC LWT cask design analyzed for the Caldecott Tunnel fire scenario does not reach internal temperatures that could result in rupture of the fuel cladding. Therefore, radioactive material (i.e., SNF particles or fission products) would be retained within the fuel rods. The potential release calculated for the NAC LWT cask in this scenario indicates that any release of CRUD from the cask would be very small - less than an A_2 quantity (see footnote 3, Section 8)

DISCLAIMER

CONTENTS

FIGURES

TABLES

APPENDIX

ABBREVIATIONS

APDL	ANSYS® Parametric Design Language
BWR	Boiling Water Reactor
CFD	Computational Fluid Dynamics
CRUD	Chalk River Unknown Deposit (generic term for various residues deposited on fuel rod surfaces, originally coined by Atomic Energy of Canada, Ltd. (AECL) to describe deposits observed on fuel removed from the test reactor at Chalk River.)
FDS	Fire Dynamics Simulator (code)
FEA	Finite Element Analysis
ISO	International Organization for Standardization (The International Organization for Standardization has decreed the use of the initials ISO for reference to the organization, regardless of the word order of the organization's name in any given language. This defines a uniform acronym in all languages.)
LWT	Legal Weight Truck
NIST	National Institute of Standards and Technology
NTSB	National Transportation Safety Board
OFA	Optimized Fuel Assembly
PNNL	Pacific Northwest National Laboratory
PWR	Pressurized Water Reactor
SFPO	USNRC Spent Fuel Project Office
SNF	Spent nuclear fuel
TFE	tetrafluoroethylene; generic term for polytetrafluoroethylene polymers such as Teflon®
USNRC	United States Nuclear Regulatory Commission

1 INTRODUCTION

Current NRC regulations specify that spent nuclear fuel shipping casks must be designed to survive exposure to a fire accident lasting at least 30 minutes, with an average flame temperature of no less than 1475°F (802°C) [1]. The cask must maintain shielding and criticality control functions throughout the fire event and post-fire cool down in order to meet USNRC requirements.

On April 7, 1982, a tank truck towing a tank trailer and carrying 8,800 gallons (33,310 liters) of gasoline was involved in an accident in the Caldecott Tunnel on State Route 24 near Oakland, California. The tank trailer overturned and caught fire. Damage to the tunnel ceiling indicated that the fire reached peak temperatures in the range of 1880-1950°F (1026-1065°C) [2]. Based on calculations for the amount of fuel present and available tunnel air flow, it is estimated that the gasoline fire burned for approximately 40 minutes, and temperatures above 1475°F (802°C) may have been sustained for up to 35 minutes during the gasoline-fueled portion of the fire [3].

The severity of the Caldecott Tunnel fire has raised questions about the performance of spent fuel casks licensed for transport by truck, should one be involved in such an accident. The staff of the USNRC Spent Fuel Project Office (SFPO) has undertaken analyses to evaluate the impact this event could have had if it had involved a spent nuclear fuel cask. As part of the investigation related to this accident, finite element analysis (FEA) evaluations were performed subjecting a model of a typical truck transportation cask to external temperatures representing the predicted conditions of this fire.

Detailed temperature boundary conditions (including temperatures of the combustion gases and the surrounding surfaces of the tunnel) were obtained from fire simulations performed at the National Institute of Standards and Technology (NIST). The purpose of this analysis of the spent fuel transport cask was to obtain an estimate of the temperature response of the various components of the cask during and after the fire.

This report presents a detailed description of the analysis, including boundary conditions, modeling approach, and computational results. Section 2 presents a brief description of the Caldecott Tunnel fire based on the National Transportation Safety Board (NTSB) investigation of the event [2]. Section 3 describes the detailed temperature boundary conditions obtained from the fire simulations performed by NIST. Section 4 describes the NAC LWT spent fuel transportation cask. Section 5 describes the analysis approach and the computational model developed for the analysis. Section 6 presents the analysis method. Section 7 describes the results of the simulation, giving a detailed evaluation of the cask response during and after the fire. Section 8 provides an analysis to determine the magnitude of any potential release of radioactive material as a consequence of the effects of the fire on the NAC LWT transportation package.

2 CALDECOTT TUNNEL FIRE EVENT

This tunnel fire occurred shortly after midnight on April 7, 1982 in Bore No. 3 of the Caldecott Tunnel on State Route 24 near Oakland, California, as the result of an accident involving a tank truck towing a tank trailer and carrying 8,800 gallons (33,310 liters) of gasoline[2]. Bore No. 3 of the Caldecott Tunnel is 3,371 ft (1027 m) long, with a two-lane roadway 28 ft (8.5 m) wide. Traffic is one-way from east to west, and the roadway has a 4% downgrade beginning approximately 30 ft (9.1 m) into the tunnel. Figure 2.1 shows a diagram of the tunnel typical cross-section. Vertical clearance between the tunnel ceiling and the roadbed is about 18 ft (5.5 m) at the center, tapering to 17 ft (5.2 m) at the side walls. The tunnel width is approximately 34.5 ft (10.5 m) between the sidewalls of the bore. The tunnel is actively ventilated by blowers with a total capacity of 1.5 million cubic feet per minute through ducting above the tunnel ceiling. (However, the blowers were not operating at the time of the fire.)

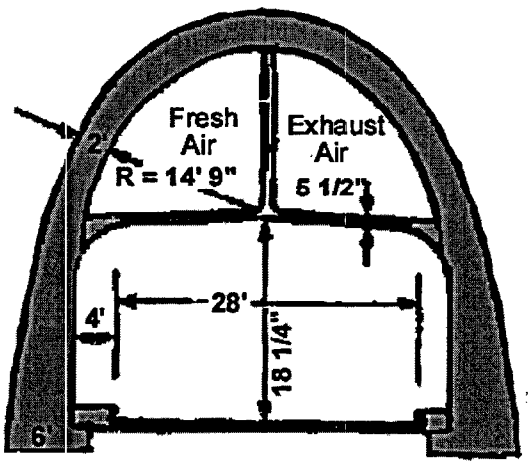

Figure 2.1. Cross-section Diagram of Bore No. 3 of Caldecott Tunnel

The roadway pavement is Portland cement concrete, as are the arched walls of the bore, which varies in thickness from 6 ft (1.8 m) at the bottom to 2 ft (0.6 m) at the top. The wall surface is covered with 4.25-inch (10.8-cm) square green tiles. The ceiling between the roadway and the ventilation ducting is 5.5-inch (14-cm) thick Portland cement concrete. Ventilation ports (5 ft x 1 ft (1.5 m x 0.3 m)) covered with steel gratings are spaced at 15-ft (4.6-m) intervals along both sides of the ceiling for the full length of the tunnel.

In the accident, the tank truck and trailer collided with a stalled vehicle in the tunnel and was subsequently struck by a bus. The tank trailer overturned and the entire vehicle (tanker and trailer) came to rest approximately 1650 ft (503 m) from the west portal of the tunnel. Gasoline spilled onto the roadway from the damaged tank trailer. A fire erupted, and within four minutes of the accident heavy black smoke began pouring out the east portal of the tunnel. The tank truck, trailer and five other vehicles in the tunnel were completely destroyed by the fire, seven persons were killed, and the tunnel incurred major damage.

Based on NTSB evaluations of the fire debris and interviews with emergency responders, the intensely hot gasoline-fueled portion of the fire is estimated to have lasted less than three-quarters of an hour. Although vehicles within the tunnel were still burning at 46 minutes after the start of the fire, firefighters in protective gear entered the tunnel to search for survivors and were able to approach the location of the tanker truck.

At approximately 55 minutes after the start of the fire, the smoke had cleared sufficiently for the CalTrans supervisor to visually assess structural damage to the tunnel and authorize fire crews to enter the tunnel. After laying hoses from the nearest standpipe in the center bore of the tunnel through cross adits (a process that required

approximately 30 minutes), the fire crews began fighting the fires due to the burning vehicles in the tunnel. Within approximately 25 minutes (about 2.7 hours after the time of the accident), these fires were reported to be "under control".

3 NIST TUNNEL FIRE MODEL

Experts at the National Institute of Standards and Technology (NIST) developed a model of the Caldecott Tunnel fire using the Fire Dynamics Simulator (FDS) code [3][1] and performed analyses to obtain predictions of the range of temperatures present in the tunnel during the fire event [4]. FDS is a computational fluid dynamics (CFD) code that models combustion and flow of hot gases in fire environments. FDS solves the mass, momentum, and energy equations for a given computational grid, and is also able to construct a visual representation of smoke flow for the fire. Full details on the analyses performed by NIST are provided in the report on the FDS analysis of the Caldecott Tunnel fire [4]. A brief description of the model and a summary of the results are presented here.

To validate the FDS code for tunnel fire applications, NIST developed fire models in FDS based on the geometry and test conditions from a series of fire experiments conducted by the Federal Highway Administration and Parsons Brinkerhoff, Inc. as part of the Memorial Tunnel Fire Ventilation Test Program [5]. NIST modeled a 6.83×10^7 Btu/hr (20 MW) and a 1.71×10^8 Btu/hr (50 MW) unventilated fire test from the Memorial Tunnel Test Program, and achieved results using FDS that were within 100°F (56°C) of the recorded data [3,6].

The NIST model of the Caldecott Tunnel for the FDS code consisted of the section of the tunnel that experienced the most severe effects of the fire. The model extends from 1509 ft to 2297 ft (460 m to 700 m) relative to the west portal of the tunnel, with the fire location defined at 1673-1706 ft (510-520 m). The fire location corresponds to the location of the tank truck and trailer, which came to rest with the front of the truck approximately 1650 ft (503 m) from the west portal. From the fire center to approximately 2297 ft (700 m), the fire resulted in essentially uniform spalling of the concrete on the tunnel walls and ceiling, the underlying reinforcing steel was exposed, and there was heat buckling of the steel ventilator opening cover plates. The wall tiles and grout also showed severe spalling in this region of the tunnel, and the fluorescent lighting fixtures and emergency phones were destroyed or damaged.

The computational grid for the tunnel fire model consisted of a fully three-dimensional (3-D) representation of this segment of the tunnel in order to capture flame and gas behavior and the interaction of the fire with the tunnel walls, ceiling, and floor. Based on boundary conditions that includes information on the available fuel and air sources, the FDS code calculates the energy release from the combustion process, the resulting flow of air and hot combustion gases, and local air and surface temperatures throughout the tunnel.

The FDS calculation simulated only the gasoline fire, and did not include the thermal energy released due to the burning vehicles. Compared to the energy released by the gasoline fire, the energy released by the burning vehicles is negligible, and these individual vehicle fires were located far from the hottest region in the tunnel. The tank truck itself was 328 ft (100 m) away from the hottest location in the tunnel during the fire. Of the five other vehicles destroyed in the fire, the closest vehicle was at least 223 ft (68 m) away from the hottest location in the tunnel, and the remaining vehicles were approximately 575 ft (175 m), and 1224 ft (373 m) away.

[1] Formal publication of the FDS code documentation began in 2001 with Version 2. Continuing validation and development of the code led to Version 3 in 2002. Version 3 was used in the FDS analyses discussed in this report.

Figures 3.1, 3.2, and 3.3 illustrate the model results, showing the evolution of the surface temperatures on the tunnel ceiling, walls and floor during and immediately after the gasoline-fueled fire. Temperature profiles are shown along the axial length of the portion of the tunnel included in the model. These plots show the surface temperature profiles along the axial length of the tunnel at the ceiling centerline (see Figure 3.1), mid-way up the tunnel wall (see Figure 3.2), and at the centerline of the tunnel floor (see Figure 3.3) at various times during the fire transient.

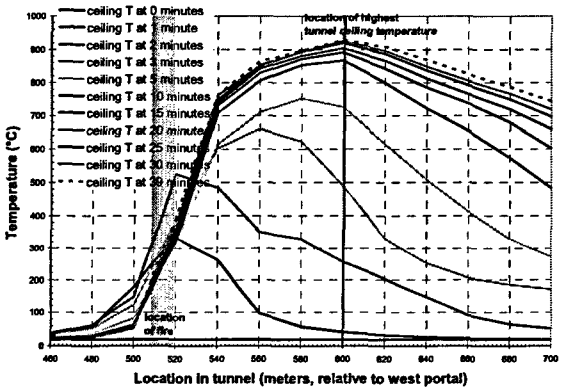

Figure 3.1. Evolution of Tunnel Ceiling Centerline Temperatures Predicted in FDS Simulation of Caldecott Tunnel Fire

The plots in Figures 3.1, 3.2, and 3.3 show that in the first few minutes of the fire, the tunnel surface temperatures in the vicinity of the fire begin to rise rapidly. Temperatures farther away down the length of the tunnel (east of the fire location) begin to rise also, but initially these temperatures rise more slowly. After about the first five minutes of the fire, however, the tunnel surfaces to the east of the fire location are rising much more rapidly than the those near the fire. By the end of the fire, at about 39-40 minutes elapsed time, the surfaces at about 262-394 ft (80-120 m) to the east of the fire (i.e., at 1968-2099 ft (600-640 m) relative to the west portal) are the hottest surfaces in the tunnel.

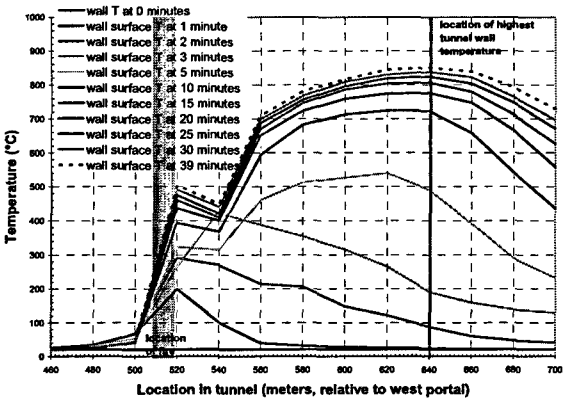

Figure 3.2. Evolution of Tunnel Wall Mid-line Temperatures Predicted in FDS Simulation of Caldecott Tunnel Fire

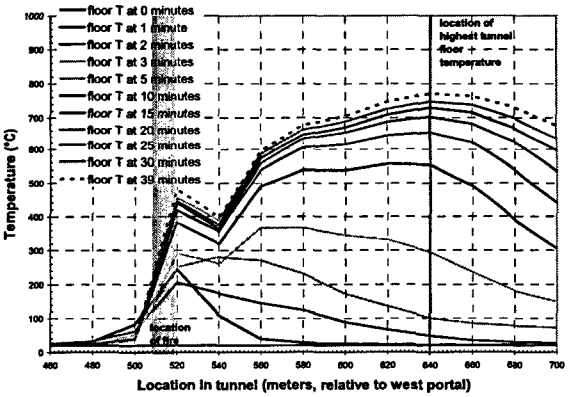

Figure 3.3. Evolution of Tunnel Floor Centerline Temperatures Predicted in FDS Simulation of Caldecott Tunnel Fire

The cause of this shift of the hottest location to a position so far from the source of the actual fire is the 'chimney' effect on the air flow through the tunnel, due to the intense heat of the fire. Expansion of combustion gases and heated air drives air flow through the tunnel, carrying the heat of the fire from east to west along the length of the tunnel. The FDS code solves for the hydrodynamics of this flow, and calculates the thermal effect on the air and surface temperatures along the length of the tunnel. Figures 3.4, 3.5,

and 3.7 show the evolution of the predicted air flow velocities in the tunnel in the upper region near the ceiling, the mid-line region near the tunnel wall, and near the floor of the tunnel.

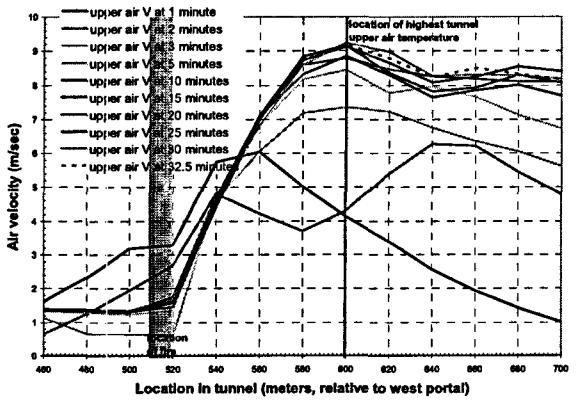

Figure 3.4. Evolution of Gas Velocity Profile near Tunnel Ceiling Centerline Predicted in FDS Simulation of Caldecott Tunnel Fire

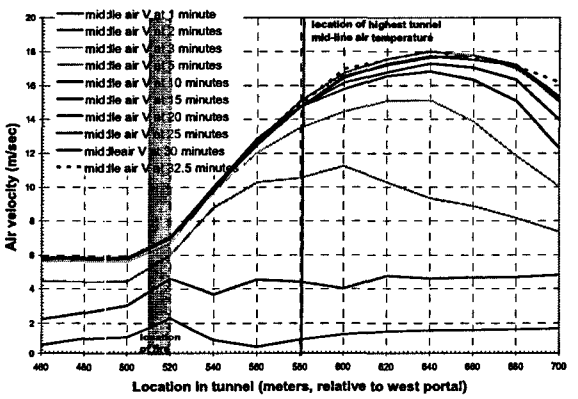

Figure 3.5. Evolution of Gas Velocity Profile near Tunnel Mid-line Predicted in FDS Simulation of Caldecott Tunnel Fire

The velocities in the plots in Figures 3.4 and 3.6 for the air near the ceiling and floor of the tunnel are from nodes approximately 1 ft (0.3 m) from their respective surfaces. The velocity in the mid-line region (in Figure 3.5) is along the tunnel centerline, mid-way between the ceiling and floor. The evolving temperature profiles for the gas moving at these velocities are shown in Figures 3.7, 3.8, and 3.9.

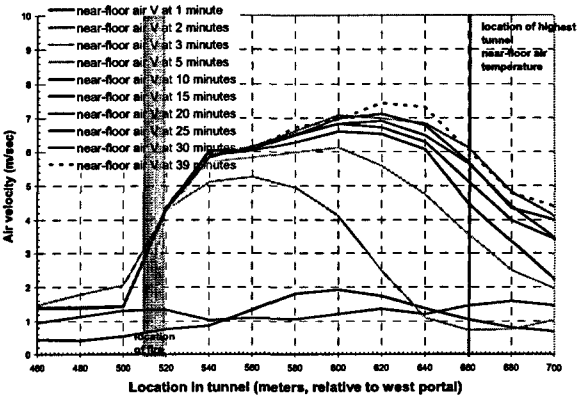

Figure 3.6. Evolution of Gas Velocity Profile near Tunnel Floor Centerline Predicted in FDS Simulation of Caldecott Tunnel Fire

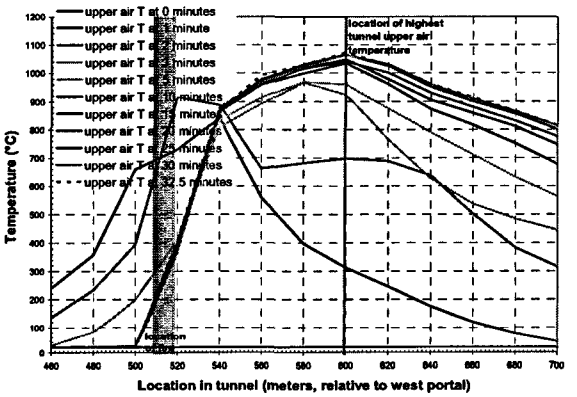

Figure 3.7. Evolution of Gas Temperature Profile near Tunnel Ceiling Centerline Predicted in FDS Simulation of Caldecott Tunnel Fire

The plots of the evolving tunnel surface temperatures in Figures 3.4, 3.5, and 3.6, and of tunnel air temperatures in Figures 3.7, 3.8, and 3.9 show that the highest temperatures during the fire

do not occur at exactly the same location in the upper, middle, and lower regions of the tunnel.

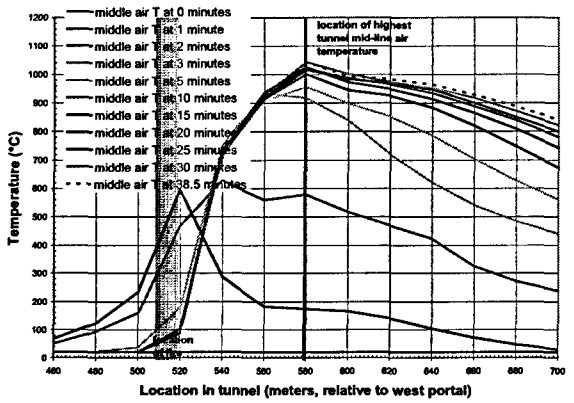

Figure 3.8. Evolution of Gas Temperature Profile near Tunnel Mid-line Predicted in FDS Simulation of Caldecott Tunnel Fire

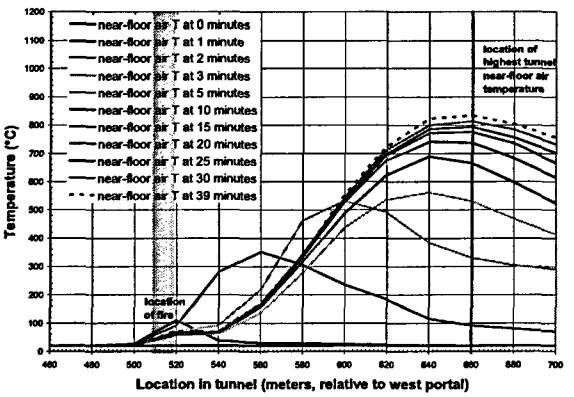

Figure 3.9. Evolution of Gas Temperature Profile near Tunnel Floor Center-line Predicted in FDS Simulation of Caldecott Tunnel Fire

Table 3.1 summarizes the peak temperatures predicted with FDS for the upper, middle, and lower regions of the tunnel. The hottest location near the ceiling of the tunnel occurs at 1969 ft (600 m), the hottest air temperature at the mid-line occurs at 1903 ft (580 m), but the hottest mid-line wall temperature occurs 197 feet (60 meters) further 'downstream', at 2100 ft (640 m). The peak air temperature near the floor also occurs at 2100 ft (640 m), but the peak floor temperature occurs at 2165 ft (660 m).

Table 3.1. Air and Surface Temperatures (°C) Near Hottest Fire Location

Location m (ft):	580 (1903)	600 (1969)	620 (2034)	640 (2100)	660 (2165)
Upper air	1039	1074	1040	985	929
Mid-line air	1042	1016	1000	982	933
Near-floor air	463	560	729	823	834
Ceiling centerline	905	935	909	869	826
Wall mid-line	789	818	844	850	839
Floor centerline	680	705	747	771	763

Nevertheless, a "hottest location" must be defined in order to determine the boundary conditions that would be seen by a nuclear fuel shipping cask subjected to the extreme temperature conditions of the Caldecott Tunnel fire. The difficulty can be resolved by considering the energy output of the fire at a given location over time, as well as the temperature history at that location. Table 3.2 summarizes the heat flux values calculated with FDS for the locations of the hottest temperatures along the tunnel.

Table 3.2: Total Energy Flux Values Near Hottest Fire Location

	energy flux (kW/hr-m^2)					
Location m (ft):	560 (1837)	580 (1903)	600 (1969)	620 (2034)	640 (2100)	660 (2165)
Ceiling centerline	106	123	134	118	100	86
Wall mid-line	61	78	89	95	96	89
Floor centerline	50	60	62	68	71	66

The highest heat flux from the fire occurs at 1969 ft (600 m) for the ceiling, and at 2100 ft (640 m) for the walls and floor. Based on the distribution of the heat output from the fire and the temperature distribution on the tunnel surfaces and in the tunnel air, the conditions at 2034 ft (620 m) give the highest temperatures at the highest heat flux values. Table 3.3 summarizes the conditions at 2034 ft (620 m), and compares the temperature and energy flux values to the peak values for the ceiling, wall, and floor regions of the tunnel.

Table 3.3: Temperature and Energy Flux Values at Hottest Location in Tunnel

Surface temperature (°C) at 2034 ft (620 m)		**% of peak**
Ceiling centerline	909	97%
Wall mid-line	844	99%
Floor centerline	747	97%
Energy flux (kW/hr-m^2) at 2034 ft (620 m)		
Ceiling centerline	118	88%
Wall mid-line	95	99%
Floor centerline	68	96%
Air temperature (°C) at 2034 ft (620 m)		
Ceiling centerline	1039	97%
Wall mid-line	1000	96%
Floor centerline	729	87%

Although none of the regions of the tunnel have their peak temperature or peak energy flux values exactly at 620 m, defining this point as the "hottest location" in the tunnel gives an overall energy flux that is within 99% of the peak energy flux, in combination with local tunnel surface temperatures that are within 1% to 3% of their respective peak values. The conditions at 2034 ft (620 m) are more severe than at 1969 ft (600 m), which has slightly higher total energy flux and wall and ceiling temperatures, but much lower tunnel floor temperatures. Similarly, the air temperatures at 2034 ft (620 m) are within 3-4% of their corresponding peak values, and although the near-floor air temperature is only 87% of its peak value at this location, at 1969 ft (600 m) it is only 67% of the peak value. In terms of the effect of the fire conditions on a cylindrical package such as a spent fuel transportation cask positioned within the tunnel, the conditions at 2034 ft (620 m) represent the best estimate of the "hottest location" in the tunnel, in that it maximizes the temperatures and heat fluxes seen by *all* surfaces of the cask.

Figure 3.10 shows the temperatures of the tunnel ceiling centerline, wall mid-line, and floor centerline predicted with FDS for the first hour of the simulation at 2034 ft (620 m), defined as the hottest location in the tunnel during the gasoline-fueled portion of the fire transient. Figure 3.11 shows the air temperatures during this time for the upper, middle, and lower regions of the tunnel at 2034 ft (620 m). Figure 3.12 shows the predicted velocities produced by the fire at the locations of the air temperatures shown in Figure 3.11. These velocities are used to define the convective heat transfer conditions on the top, sides and bottom of the spent fuel cask during the fire. (The temperature-vs.-time and velocity-vs.-time values in these plots were smoothed to conservatively remove the rapid stochastic variations typical of fire dynamics, preserving only the major peaks and troughs defining the general physical behavior of the simulated fire.)

Maximum gas temperatures calculated in the FDS model are on the order of 1965°F (1074°C). The maximum tunnel surface temperatures are predicted to be only about 1715°F (935°C) (see Figure 3.10). Maximum air temperatures in the upper and middle regions of the tunnel are predicted to exceed 1832°F (1000°C) in the first 5 to 6 minutes of the fire, and remain above this temperature until the end of the gasoline-fueled portion of the fire (at approximately 40 minutes.)

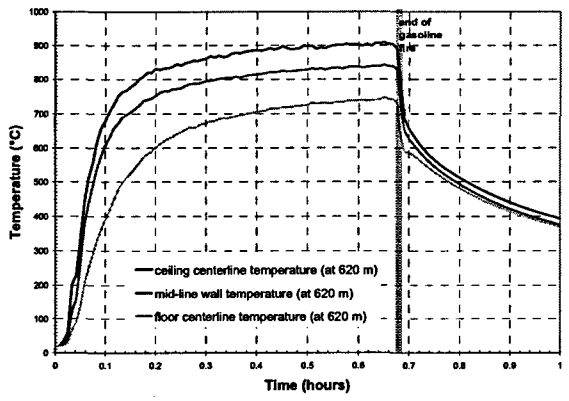

Figure 3.10. Tunnel Surface Temperatures at Hottest Location Predicted for First Hour of FDS Simulation of Caldecott Tunnel Fire

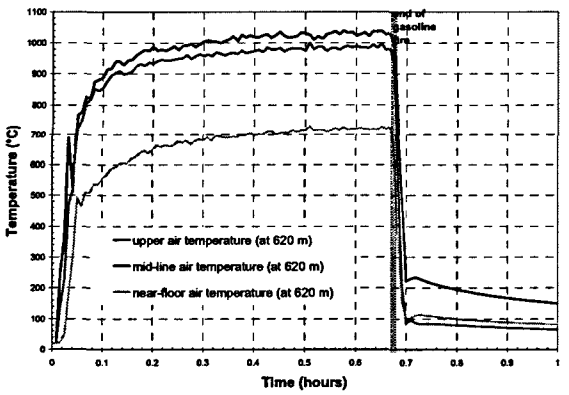

Figure 3.11. Tunnel Air Temperatures at Hottest Location Predicted for First Hour of FDS Simulation of Caldecott Tunnel Fire

The FDS calculation was run out for a total transient time of three hours, including the 40-minute gasoline-fueled fire and a 2.3 hr cool-down period. Temperatures and velocities for the full duration of the FDS calculation are shown in Figure 3.13 (for the tunnel surface temperatures), Figure 3.14 (for the tunnel air temperatures), and Figure 3.15 (for the tunnel air velocities.) By the end of this three-hour period, the tunnel air temperatures predicted at the hottest location have dropped to 154°F (68°C) or lower, and the tunnel surface temperatures are less than 320°F (160°C)

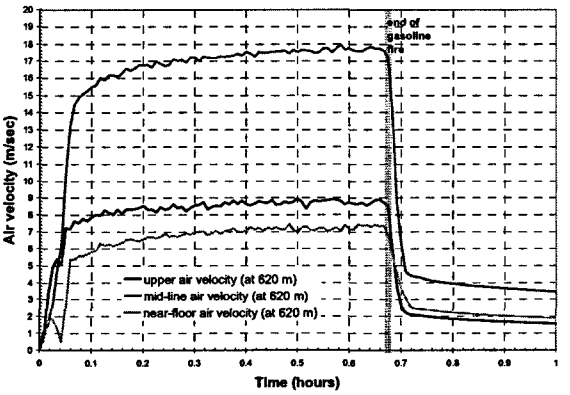

Figure 3.12. Tunnel Air Velocities at Hottest Location Predicted for First Hour of FDS Simulation of Caldecott Tunnel Fire

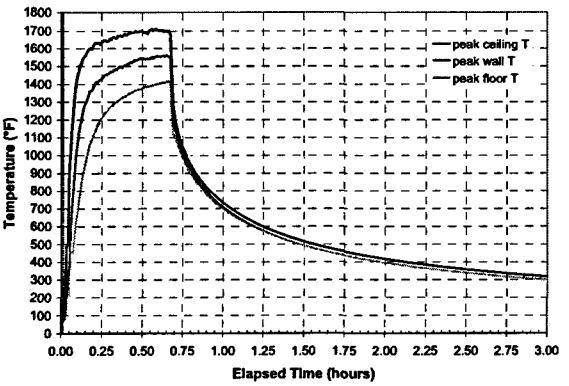

Figure 3.13. Peak Tunnel Surface Temperatures Predicted in 3-Hour FDS Simulation of Caldecott Tunnel Fire

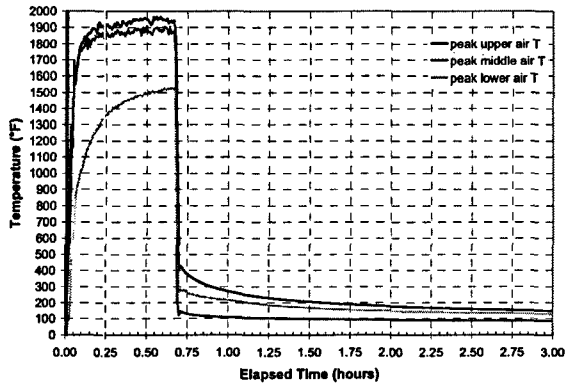

Figure 3.14. Peak Tunnel Gas Temperatures Predicted in 3-Hour FDS Simulation of Caldecott Tunnel Fire

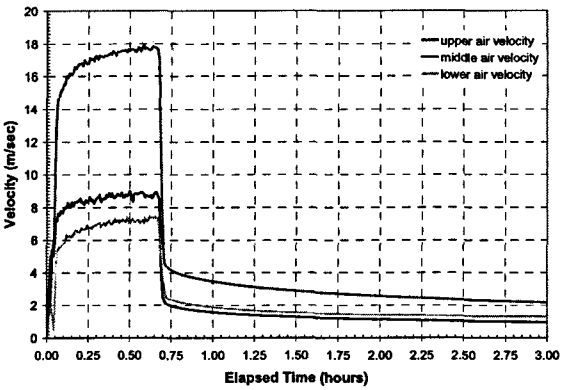

Figure 3.15. Peak Tunnel Gas Velocities Predicted in 3-Hour FDS Simulation of Caldecott Tunnel Fire

4 TRANSPORTATION OF SPENT NUCLEAR FUEL

NRC regulations require spent fuel transportation packages to be evaluated for a series of hypothetical accident conditions that include a fully engulfing fire with an average flame temperature of 1475°F (802°C) for a period of 30 minutes. The certification process must include either an open pool fire test or an analysis of the package for a fire exposure meeting these criteria. Packages must maintain shielding and criticality control functions throughout the sequence of hypothetical accident conditions.

In this investigation, a typical spent nuclear fuel transportation package licensed for over-the-road transport by truck is subjected to boundary conditions simulating the thermal conditions of the Caldecott Tunnel fire, to determine the response of the package to these severe conditions. The Nuclear Assurance Corporation (NAC) Legal Weight Truck (LWT) transportation package was selected for this analysis because it represents a typical package that can be transported by truck. A complete description of the package design and loading configurations can be found in the licensing SAR [7]. A brief description of this design is presented below.

4.1 NAC LWT Transport Package

The NAC LWT transportation package is certified to be carried on a standard tractor trailer truck. It is typically shipped within an International Organization for Standardization (ISO) shipping container. Figure 4.1 shows a picture of an LWT package on a flat-bed trailer with a personnel barrier installed, but without an ISO container. Figure 4.2 shows an exterior view of the package within an ISO container on a flat-bed trailer. This package is designed to transport a variety of commercial and test reactor fuel types with widely varying maximum decay heat load specifications. For this analysis, the cask was assumed to contain a single PWR spent nuclear fuel assembly, with a decay heat load of 8,530 Btu/hr (2.5 kW). This is the highest heat load the LWT package is rated for with any spent fuel it is designed to carry (refer to Amendment 34 of the SAR [7]), and ensures a conservative thermal load for the package in the fire accident scenario.

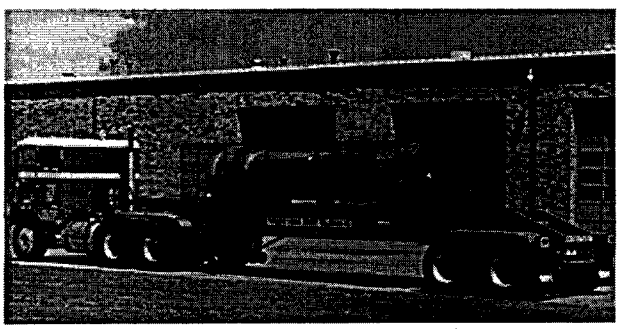

Figure 4.1. NAC LWT Transport Package (without ISO container)

Figure 4.2. NAC LWT Transport Package (with ISO container)

The loaded package weighs approximately 52,000 lb (23,586 kg). The containment boundary provided by the stainless steel package consists of a bottom plate, outer shell, upper ring forging, and closure lid. This cask has an additional outer

stainless steel shell to protect the containment shell, and also to enclose the lead gamma shield. Neutron shielding is provided by a stainless steel neutron shield tank containing a water/ethylene glycol mixture. An additional annular expansion tank for the mixture is provided, external to the shield tank. This component is strengthened internally by a network of stainless steel stiffeners. Aluminum honeycomb impact limiters covered with an aluminum skin are attached to each end of the cask during transport. The entire package, including impact limiters, fits within an ISO container, which is constructed of steel plate.

5 ANALYSIS APPROACH

In the analytical approach used to evaluate the response of the NAC LWT transportation cask to the conditions of the Caldecott Tunnel fire, a highly detailed three-dimensional (3-D) model was constructed. The ANSYS [8] general finite element analysis (FEA) package was selected for this analysis, since it is a widely used analytical tool for licensing analyses of spent nuclear fuel casks. Using this approach, the model included all significant heat transfer paths within the cask and between the cask and the external environment. The computational model was subjected to the thermal environment of the tunnel during the fire transient using boundary conditions derived from the NIST simulation of the fire using FDS computational fluid dynamics code.

The model of the NAC LWT cask constructed for ANSYS consists of a detailed 3-D representation of a symmetric half-section of the spent fuel package and a complete cross section of the surrounding tunnel wall. Because the cask can be shipped uncovered or enclosed in an ISO shipping container, two models were constructed; one that included the ISO container, and one that did not. For both cases, the cask is oriented horizontally within the tunnel. This orientation gives the cask or ISO container outer surface the maximum exposure to the highest temperatures in the fire environment. This includes exposure to the tunnel surfaces for thermal radiation exchange and to the flow of hot gases generated by the fire, which results in significant convection heat transfer to the package during the fire transient. A diagram of the package model (including the ISO container) and part of the tunnel is shown in Figure 5.1. Figure 5.2 shows a similar diagram for the analysis without the ISO container.

The flatbed of the truck, which would tend to shield the bottom of the cask from the effects of the fire, is omitted from the analysis. However, the cask is assumed to be located within the tunnel at a vertical height corresponding to the height of the flatbed. This assumption yields the minimum possible distances for thermal radiation exchange with the hottest surfaces in the tunnel environment, and exposes the cask to the hottest air temperatures in the tunnel.

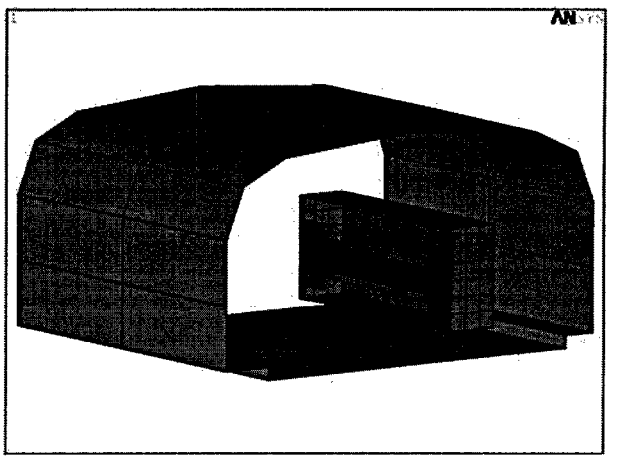

Figure 5.1. ANSYS NAC LWT Cask Analysis Model Element Plot (with ISO)

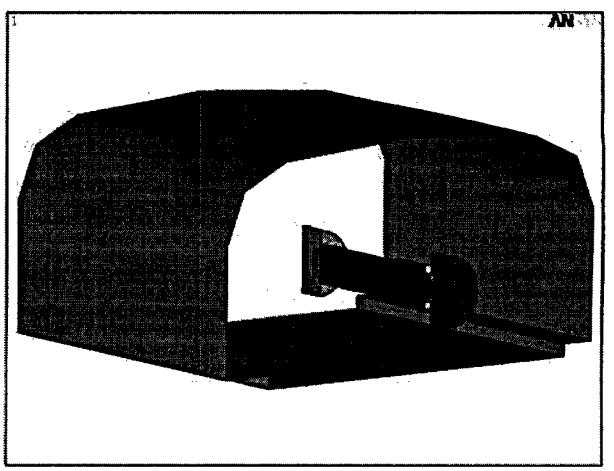

Figure 5.2. ANSYS NAC LWT Cask Analysis Model Element Plot (without ISO)

The model used 40,489 SOLID70 8-node brick elements and 4,776 SHELL57 4-node quadrilateral thermal elements to represent the structural components. A total of 7,165 SURF152 elements were used to include thermal radiation between the ISO container surfaces and the tunnel, and convection heat transfer at the ISO container surfaces. Sixteen MATRIX50 elements were used to model thermal radiation exchange between surfaces within the ISO container. The surface effect elements were also used to generate solar insolation loads for calculation of the initial steady-state temperature distribution for the cask.

5.1 Model of NAC LWT Transportation Package

The model geometry for the internal components of the cask was developed from the vendor's engineering drawings. The representation of the cask internal components was identical in both cases considered, with and without the ISO container enclosing the cask. The cask contains a cylindrical solid aluminum basket that holds a single fuel assembly. The helium gaps between the fuel and the basket, and between the basket and cask shell, were explicitly modeled with solid elements. The cask model cross section is shown in Figure 5.3.

The cask body is constructed of concentric stainless steel shells to provide structural support and some gamma shielding. The innermost shell is surrounded by a layer of lead that acts as the main gamma shield. The outermost stainless steel shell is surrounded by an annular tank containing a 56% solution of ethylene glycol and water which acts as a neutron shield. The tank is contained by an outer stainless steel skin and an annular overflow tank that extends approximately one-third the axial length of the cask body.

All of these components were modeled using brick elements. The tank is constructed with sixteen stainless steel support ribs connecting the skin to the outer shell. These structures were modeled with shell elements.

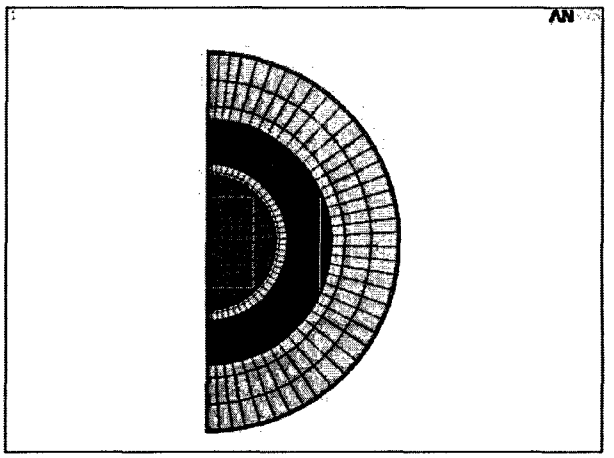

Figure 5.3. Cross Section of NAC LWT Cask Model in ANSYS

The cask bottom consists of a stainless steel base, a layer of lead shielding, and a steel cover. The upper end of the cask is sealed with a stainless steel lid, as illustrated in Figure 5.4. Impact limiters attached to each end of the cask consist of an internal aluminum honeycomb structure covered by an aluminum skin. The expansion tank to handle overflow of the liquid neutron shield has an outer stainless steel skin.

In the ANSYS model, the cask is assumed to be located relative to the tunnel surfaces at a level corresponding to the height it would be above the tunnel floor when sitting on the bed of the truck. For the analysis in which the cask is within an ISO container, it is similarly assumed that the top of the ISO container is at a height corresponding to the height of the container plus the height of the truck bed.

All three possible modes of heat transfer (i.e., conduction, convection, and radiation) were carefully represented in the model for thermal energy exchange between all of the components.

Conduction is handled inherently by the geometry of the connections between the elements modeling each component, but convective and radiation mechanisms must be carefully implemented using appropriate modeling options.

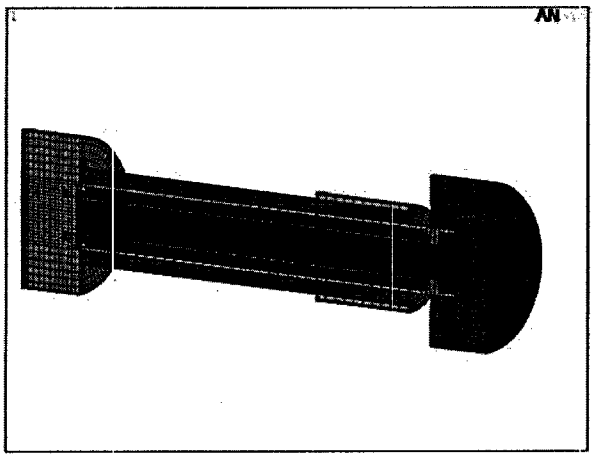

Figure 5.4. NAC LWT Cask Geometry

Westinghouse 17x17 OFA fuel was used in this evaluation. The fuel assembly was modeled with an effective conductivity determined using a homogenization scheme similar to that presented by Bahney and Lotz [9], modified to include a helium gap between the homogenized fuel region and the fuel basket. This yields a more realistic representation of the temperature profile through the assembly, and takes into account the effect of the non-uniform wall temperature distribution around the assembly.

Axial conduction in the homogeneous fuel region was conservatively neglected in the fuel itself, and was modeled in the cladding only, using the conductivity of Zircaloy modified by a weighting scheme based on the cross-sectional area. The effective density and heat capacity for the fuel region was based on volumetric averages of the properties of the helium cover gas, fuel rod cladding, and uranium oxide fuel pellets. The design basis axial power profile from the SAR [7], which has a normalized peaking factor of 1.2, was used to establish the volumetric heat generation of 8,532 Btu/hr (2.5 kW) over the active fuel length of the assembly.

The 0.225-inch (0.57-cm) gap filled with a helium cover gas between the fuel and the basket was modeled with solid elements and used standard helium thermal conductivity, density, and specific heat. Convection was ignored in this small gap. The 0.25-inch (0.64-cm) gap between the basket and the inner shell was modeled in the same manner, assuming negligible convection. Gaps between the lead gamma shielding and cask inner and outer shells due to contraction of the lead after pour were accounted for in the model by computing effective conductivities assuming both thermal radiation and conduction across the gap. Effective conductivities were also used to include the effect of the Fiberfrax paper insulation between the lead and the steel cask shell.

Radiation interaction across helium-filled enclosures in the cask interior was modeled by coating the surfaces of elements bordering these regions with SHELL57 elements having specified emissive material properties. The SHELL57 elements were then used to produce highly structured AUX-12 generated MATRIX50 superelements, each defined by an enclosure, and the AUX-12 hidden ray-tracing method was used to compute view factors for each element in the superelement. A total of 10 MATRIX50 superelements were defined to capture the thermal radiation interactions within the cask and canister.

5.2 NAC LWT Transportation Package within the Tunnel

The presence or absence of the ISO container has a significant effect on the environment seen by surface of the LWT cask within the tunnel. Without the ISO container, the exterior surface of the cask is directly exposed to the tunnel environment during the fire. With the ISO

container, the exterior surface of the cask is shielded from direct interaction with the tunnel environment. Instead, the cask exchanges heat with the inner surface of the ISO container, and only the ISO container outer surface is directly exposed to the tunnel environment. As a result, the two cases require somewhat different modeling approaches to appropriately account for heat transfer at the cask surface.

5.2.1 With ISO Container

For the analysis with the cask enclosed in an ISO container, the model illustrated in Figure 5.4 was enclosed within additional elements modeling the ISO container, as shown in Figure 5.5. For the large air volumes between the cask outer surface and the inner surface of the ISO container, conduction across the gaseous medium is negligible, but significant convection currents will be created by the buoyant forces due to the heated surfaces. Surfaces with unobstructed views of other surfaces will also experience significant radiation exchange that is highly dependent on the surface geometry. Therefore, heat exchange between the cask exterior and the container interior was modeled with internal free convection and thermal radiation between interior surfaces.

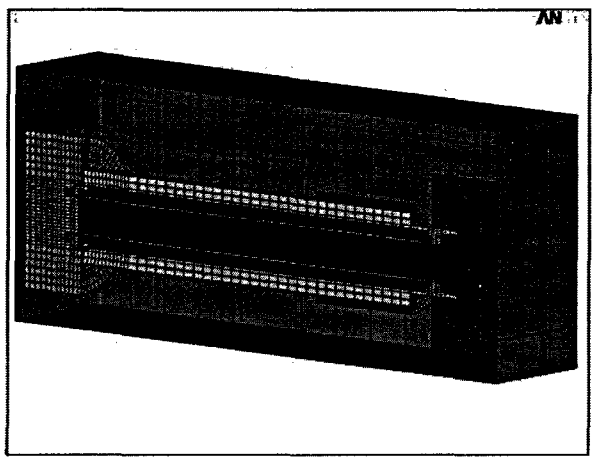

Figure 5.5. NAC LWT Cask Geometry within ISO Container

Calculations for convection heat transfer on the external surface of the ISO container used empirical relations for free convection over flat plates (see Section 6 for full details). Convection at a surface was implemented using SURF152 elements. These elements are placed on the exterior surface of a body and communicate with the designated sink temperature assigned to a single node (called the "space node") to compute the heat flux.

Convective heat transfer rates between the outer surface of the cask and the inner surface of the ISO container are expected to vary in different regions, due to geometry considerations and varying temperature gradients. This was accounted for in the model by dividing the volume enclosed by the ISO container into 17 zones, as illustrated in Figure 5.6. A separate zone was defined on each end of the cask, three zones were defined for the top, side, and bottom radial surfaces of each impact limiter, and three similar zones were defined for the cask body along its axial length. The sink temperature for each zone is computed as the average surface temperature of the participating cask surface elements and ISO container inner surface elements for that zone.

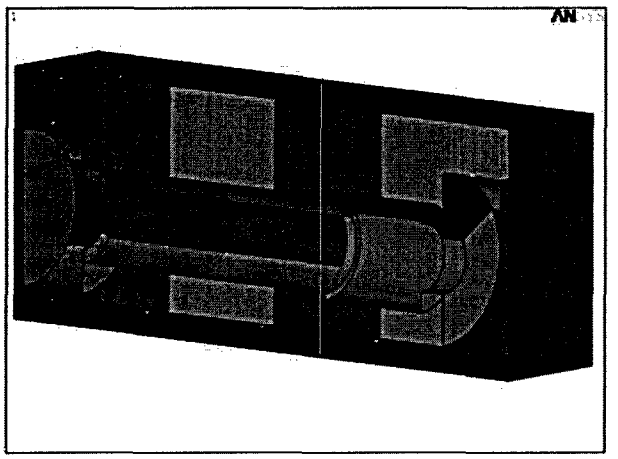

Figure 5.6. Zones for Convection Computations Within the ISO Container

A convective heat transfer coefficient is assigned to the cask and container elements based on the surface geometry and the temperature difference between the surface and the local sink temperature for that zone (see Section 6.)

In addition to convection heat transfer at the cask surface, a total of five MATRIX50 superelements were defined to capture the radiation interaction between the cask and interior surfaces of the ISO container. The heat exchange between these surfaces and the space node is computed by ANSYS during the solution.

Convection and thermal radiation are also the two available mechanisms for heat transfer from the exterior surface of the ISO container. In the fire analysis, the initial temperature distribution is obtained from a steady-state calculation for boundary conditions specified by 10CFR71.71 [1], followed by a transient calculation representing the fire.

During the fire, the sink node temperatures for the SURF152 elements are set and the external convection coefficient is computed using a forced convection relation derived from gas temperatures and velocities predicted in the NIST fire simulation. These results were obtained for the top, side, and bottom of the tunnel, and applied to three zones defined on the top, sides, and bottom of the ISO container, as illustrated in Figure 5.7.

Thermal radiation between the outer surface of the ISO container and the tunnel during and after the fire is incorporated by a MATRIX50 element, as described above for radiation exchange between surfaces within the cask. The top, side, and bottom temperatures in the tunnel predicted in the NIST fire simulation with FDS are imposed as boundary conditions on the elements modeling the tunnel surfaces. Emissivity values of 1.0 for the tunnel surfaces and 0.9 for the ISO container exterior surfaces were used, on the assumption that these surfaces would be severely blackened during the fire due to the effect of sooting.

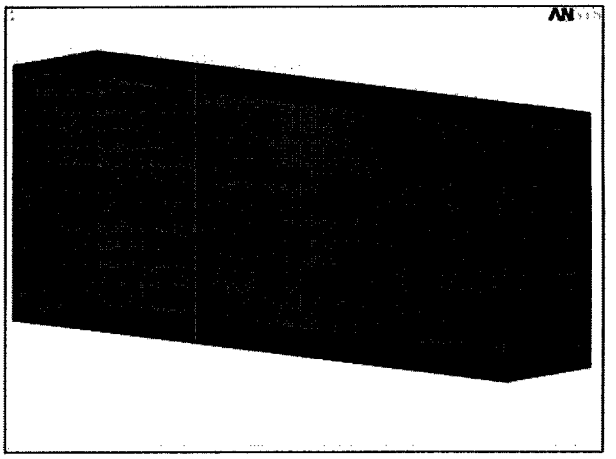

Figure 5.7. Zones for External Heat Transfer Between ISO Container and Tunnel

5.2.2 Without ISO Container

For the analysis of the cask without an ISO container, the cask model illustrated in Figure 5.4 was connected directly to the tunnel environment. Calculations for convection heat transfer on the external surface of the cask were based on empirical relations for convection over cylinders (see Section 6 for full details). Convection at a given surface was implemented using SURF152 elements, in essentially the same manner as described above for the external surfaces of the ISO container.

Similarly, radiation interaction between the cask outer surface and the tunnel was established by coating all respective interacting surfaces with SHELL57 elements with specified emissive material properties. The SHELL57 elements were then used to produce a highly structured AUX-12 generated MATRIX50 superelement.

The top, side, and bottom temperatures in the tunnel predicted in the NIST fire simulation with

FDS are imposed as boundary conditions on the elements modeling the tunnel surfaces. Emissivity values of 1.0 for the tunnel surfaces and 0.9 for the LWT cask exterior surfaces were used, on the assumption that these surfaces would be severely blackened during the fire due to the effect of sooting.

5.3 NAC LWT Transportation Package Material Properties

The material thermal properties used in the analytical model (with and without the ISO container) were obtained from the vendor's SAR [7] and are listed in Appendix A. Some modifications were made to the material properties to account for structural configuration changes and expected effects of the fire. For the aluminum honeycomb material, the significant void volume reduces the heat transfer capability compared to solid material. The thermal conductivity assigned to the impact limiters was scaled by the ratio of the honeycomb density to the solid aluminum density.

Modeling of the liquid neutron shield was complicated by the expectation that the 56% ethylene glycol liquid will exceed its boiling point during any fire simulation. This can be expected to lead to tank rupture and vaporization of the contents, which significantly affects the heat transfer behavior of the cask. Prior to rupture, the liquid in the tank is expected to sustain convection currents due to temperature gradients through the liquid between the tank surfaces. After rupture, empirical relations were used to obtain separate effective conductivities for the shield tank and expansion tank. (Refer to Section 6 for details on correlations used in this approach.)

The effective conductivity was determined as a function of the average tank temperature and the radial temperature difference between the tank inner and outer surfaces. The material properties were updated between each time step during the transient solution using ANSYS® Parametric Design Language (APDL). The affected nodes were assumed to consist of a 56% ethylene glycol solution up to the point where the average temperature reached the mixture's boiling point of 350°F (177°C).

When the average temperature in the tank exceeded the boiling point, it was assumed that rupture occurred and the liquid was immediately vaporized. The effective conductivity was then computed using air as the medium. This calculation was continued during the cool down period also. This formulation conservatively neglects energy absorbed by the phase change (i.e., the heat of vaporization for the liquid), but mainly as a matter of convenience, since this would constitute a very small deduction from the total energy imparted to the cask. After rupture, thermal radiation exchange within the empty tanks was also activated using MATRIX50 superelements.

6 ANALYSIS METHOD

Analyses have been performed by the National Institute of Standards and Technology (NIST) using various assumptions related to the type of fire that could have been sustained in the Caldecott Tunnel. Results from the NIST analyses, including temperature and flow predictions for the postulated fire and post-fire scenario, were used to develop the boundary conditions applied to the ANSYS model of the NAC LWT cask.

Section 6.1 lists the conservative assumptions underlying the analytical approach used. Section 6.2 describes the boundary conditions derived from the NIST simulation with FDS, and defines their application to the ANSYS analysis of the NAC LWT cask. This includes temperature boundary conditions and the approach used to define convection and radiation heat transfer rates, and the methods used to account for material degradation during the fire. Section 6.3 describes the initial steady-state conditions for the NAC LWT cask model, with and without the ISO container, at the beginning of the fire transient. Section 6.4 describes the procedure used for the transient calculations.

6.1 Modeling Assumptions for Fire Transient

A number of conservative assumptions were made in developing models and performing evaluations of the thermal response of the NAC LWT spent fuel transport package to the Caldecott Tunnel fire transient. The assumptions of greatest impact are listed below.

1) Boundary conditions were taken from the hottest location within the tunnel, which was determined to be 2034 ft (620 m), which is 328 ft (100 m) to the east (downstream) of the location of the fire, based on predictions of peak gas temperatures in the lower, middle, and upper zones of the tunnel, and peak surface temperatures and energy fluxes on the tunnel floor, walls, and ceiling.

2) The peak temperature values in each region were used to define boundary temperatures over the entire region, rather than using the detailed local temperature distributions predicted in the FDS calculation. This approach ensures a conservative estimate of the boundary temperatures, since the package does not see the peak temperatures on all surfaces, and in some cases may not see the peak temperature on any surface. (For example, the top of the package is not high enough to be directly exposed to the peak gas temperature near the top of the tunnel, but this value was used as the ambient temperature for convective heat transfer to the upper surface of the package.)

3) The package cradle and the trailer bed were omitted from the ANSYS model of the NAC LWT package. These structures were neglected because they could partially shield the package from thermal radiation from the hot tunnel surfaces or block convection heat transfer to the package due to the flow of hot gas generated by the fire. This approach eliminated any potential shielding of the package from thermal radiation and convection heat transfer from the tunnel environment.

4) During the simulated gasoline-fueled fire ($t <$ 0.7 hr) and the short-term post-fire cool down period (0.7 hr $< t <$ 3.0 hr), it was assumed that forced convection heat transfer at the outer surface of the package was due solely to air flow induced in the tunnel by the temperature gradients of the fire. Convection heat transfer

rates were calculated using the gas velocities at the locations of the peak gas temperatures, as predicted in the NIST analysis with FDS. This approach neglects the possible contribution of additional heat transfer from the package due to free convection resulting from vertical temperature gradients around the package. This boundary condition was switched to solely free convection after 3.0 hours, in the extrapolated extended cool down portion of the transient. This conservatively neglects any forced convection cooling of the package during the extended cool down period, when the gas velocities in the tunnel are predicted to have dropped to relatively small values.

5) Attenuation of thermal radiation during the fire due to optical densification (i.e., smoke and particulates from combustion and material degradation) was not taken into account in the transient calculation. However, because the fire was reported to have produced thick black smoke, it was assumed that the outer surfaces of the package would 'see' the peak gas temperatures for thermal radiation exchange, rather than the tunnel surface temperatures. This provides a conservative treatment of heat transfer due to thermal radiation, since the FDS calculation predicted that the gas temperatures would be higher than the tunnel surface temperatures during and shortly after the fire. For the analysis with the cask within an ISO container, attenuation of thermal radiation was also neglected between the cask and inner surfaces of the ISO container. In these regions, radiation views were treated as clear and unobscured at all times during the transient.

6) Materials that would burn, boil off or melt during the transient were assumed to remain intact during the fire. At the end of the fire, the thermal conductivity values for these materials were reduced to that of air. The higher thermal conductivity values of the intact material tends to maximize the heat input into the package during the fire. When these values are replaced with the thermal conductivity of air, the affected components present an added thermal barrier to heat removal from the package after the fire. In addition, the energy absorbed by these materials, due to latent heat of fusion or vaporization, was not subtracted from the energy input to the package from the fire.

Given these assumptions and the extremely detailed 3-D model of the spent fuel transportation package, the ANSYS analyses presented here constitute a conservative evaluation of the response of the NAC LWT cask to the Caldecott Tunnel fire scenario. The boundary conditions from the FDS simulation of the Caldecott Tunnel are presented in Sections 6.2 through 6.4.

6.2 Boundary Conditions for Fire Transient

Boundary conditions from the NIST simulation with FDS were selected from a location approximately 328 ft (100 m) downstream of the fire source. This location corresponds to the hottest gas temperatures and highest thermal energy output of the fire (see the discussion in Section 3 and the plots in Figures 3.13, 3.14, and 3.15.) Section 6.2.1 describes the tunnel surface temperatures and gas temperatures selected to define the boundary conditions for the ANSYS calculation. Section 6.2.2 describes the heat transfer boundary conditions applied in the analysis, based on the gas temperatures and associated gas velocities.

6.2.1 Boundary Temperatures from FDS Analysis

Peak tunnel surface temperatures, peak gas temperatures, and associated gas velocities over time from the NIST simulation with FDS were

selected from a location approximately 328 ft (100 m) downstream of the fire source. As a conservative simplification of the finely detailed meshing of the fluid nodes in the FDS simulation, the tunnel air volume was divided into three sections, consisting of an upper, middle and lower region. As an additional simplification, the analysis neglected the shielding effect of cask mounting structures and the trailer bed supporting the package above the roadway.

The regions were defined based on the geometry of the tunnel and the position of the package within the tunnel. The upper region was defined as the tunnel volume extending from the tunnel ceiling to 15.3 ft (4.7 m) above the tunnel floor. The middle region was defined as the volume extending from 15.3 ft (4.7 m) to 1.0 ft (0.3 m) above the tunnel floor. The lower region was defined as the volume between the tunnel floor and 1.0 ft (0.3 m) above the tunnel floor. The tunnel surfaces in the ANSYS model were divided into three corresponding regions; ceiling, side walls, and floor. The upper region consists of the ceiling and upper wall to 15.3 ft (4. 7 m) above the tunnel floor. The middle region consists of the tunnel wall from 15.3 ft (4.67 m) to 1.0 ft (0.3 m) above the tunnel floor. The lower region consists of the tunnel floor and up the wall to 1.0 ft (0.30 m) above the tunnel floor.

Rather than tracking the local surface and gas temperatures, and gas velocities, predicted over the fine mesh within each of these regions in the detailed NIST simulations with FDS, the boundary temperatures used in the ANSYS calculations were defined by applying the peak temperature and velocity values in a given region over the entire region. Within a given region, the predicted peak tunnel surface temperature, peak gas temperature, and associated gas velocity as a function of time were used to defined the boundary conditions for the entire region.

Using this conservative simplification, boundary temperatures were specified for the top region, side region, and bottom region of the ANSYS model of the package within the tunnel. For the analysis with the ISO container, the top region consists of the upper surface of the ISO container, the side region consists of the three vertical surfaces of the half-section of symmetry of the ISO container, and the bottom region of the model consists of the ISO container base.

For the analysis without the ISO container, the top region consists of the upper 60-degree arc of the 180-degree half-section of symmetry of the cask circumference. The bottom region consists of the lower 30-degree arc of the cask circumference, and the side region consists of the 90-degree arc between the upper and lower region. This division was also applied to the impact limiters.

In clear air, the cask surfaces (without the ISO container) or the ISO container surfaces would see the tunnel surfaces for radiation exchange. However, during the fire portion of the transient, this view is obscured due to smoke and other combustion gases filling the tunnel. This means that the package would see the gas temperature rather than the wall temperature for radiation heat transfer. This is significant, since during the fire portion of the transient, the peak gas temperatures from the upper and middle regions of the tunnel are generally 180-270°F (100-150°C) above the peak ceiling and wall surface temperatures (as can be seen from Figures 3.10 and 3.11).

This is represented in the ANSYS simulations by specifying the gas temperatures rather than the tunnel surface temperatures as the temperatures seen by the package outer surfaces for thermal radiation heat transfer during the fire. After the fire, the smoke was reported to have cleared out fairly rapidly, so that in a relatively short time, the package surfaces would be expected to see the tunnel surfaces. This transition was modeled by

selecting the boundary temperature as the higher of the tunnel surface temperature or gas temperature for the given region.

In practical terms, this means that the radiation boundary temperature for a region switches from the gas temperature to the tunnel surface temperature very shortly after the end of the fire. Figure 6.1 shows the boundary temperatures for thermal radiation for each region, which were selected as the maximum of the gas temperature or the surface temperature for the corresponding region of the tunnel.

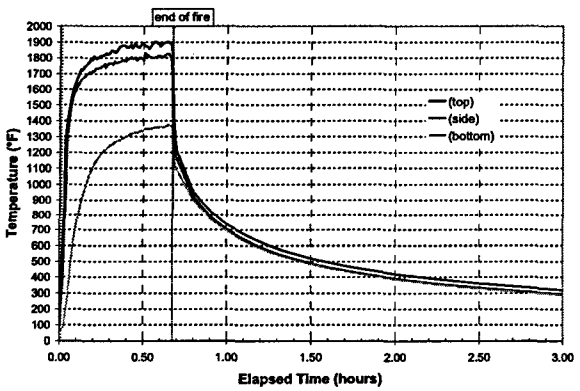

Figure 6.1. Peak Temperatures for Radiation Exchange During Fire Transient in Caldecott Tunnel

The boundary temperatures for convection heat transfer in each region is shown in Figure 6.2. In all regions, this temperature is the corresponding peak gas temperature from the NIST calculation with FDS. The gas velocities used in each region are also taken from the NIST calculation, at the location of the corresponding peak temperature. These velocities are shown for each region in Figure 6.3. These temperature-vs.-time and velocity-vs.-time values used as boundary conditions in the ANSYS calculation were smoothed to conservatively remove the rapid stochastic variations typical of dynamic fire behavior, preserving only the major peaks and troughs related to the general physical behavior of the simulated fire.

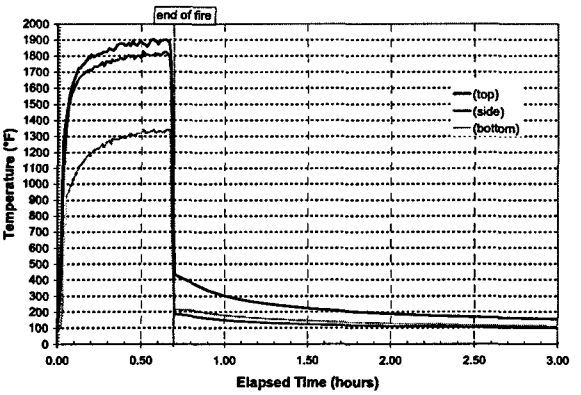

Figure 6.2. Peak Temperatures for Convection Heat Transfer During Fire Transient in Caldecott Tunnel

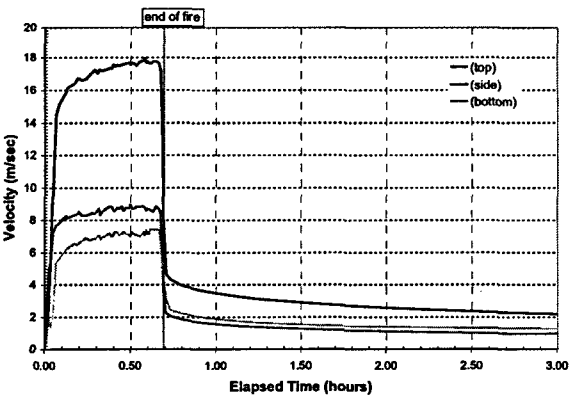

Figure 6.3. Peak Velocities for Convection Heat Transfer During Fire Transient in Caldecott Tunnel

The FDS analysis performed by NIST was carried out for a 40-minute gasoline-fueled fire and 2.3-hour post-fire cool-down, for a total simulation duration of 3 hours. To determine the complete time and temperature response of the package, and explore the effects of prolonged exposure to post-fire conditions in the tunnel, the ANSYS analysis extended the post-fire cool down to 50 hours. Tunnel surface and gas temperatures predicted

with FDS at 3 hours were extrapolated from 3 hours out to 50 hours using a power function, to realistically simulate cool down of the tunnel environment.

Figures 6.4 and 6.5 show the boundary temperatures for radiation and convection heat transfer, respectively, extrapolated from 3 hours out to 50 hours. The extrapolation was performed by fitting a power function to the post-fire portion of each of the boundary temperature curves from the FDS simulation, such that

$$T_n = a_n t^{b_n}$$

where

T_n = extrapolated boundary temperature of region n

a_n = leading coefficient of regression fit to boundary temperature curve n

b_n = exponential coefficient of regression fit to boundary temperature curve n

t = elapsed time

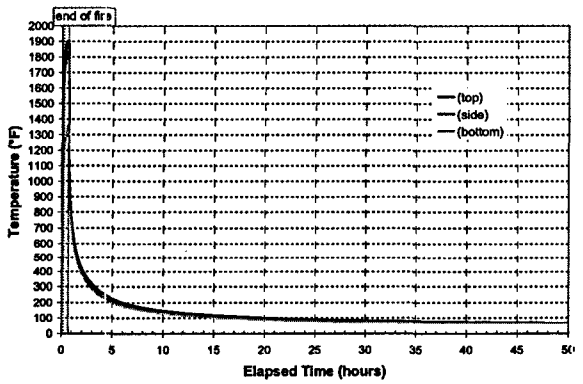

Figure 6.4. Peak Temperatures for Radiation Exchange During Extended Transient in Caldecott Tunnel

By three hours into the transient (2.3 hr after the end of the simulated fire), the predicted gas velocities for forced convection have dropped to less than 2 ft/s (0.6 m/s). At that time, the convection heat transfer boundary at the package surface is switched from forced convection to free convection only. By 50 hours, the extrapolated boundary conditions predict that the peak gas temperatures and surface temperatures in the tunnel will be back to the normal tunnel ambient air temperature of 68°F (20°C), and all boundary temperatures are essentially constant.

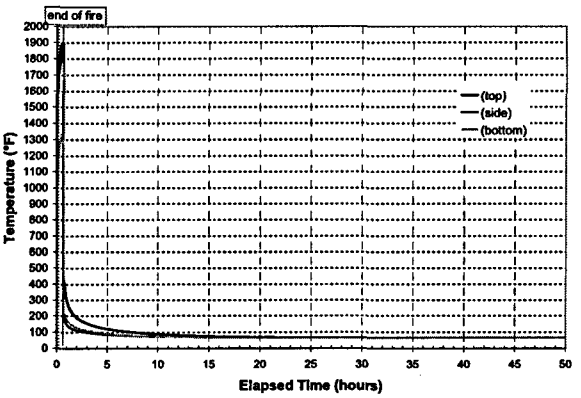

Figure 6.5. Peak Temperatures for Convection During Extended Transient in Caldecott Tunnel

6.2.2 Convection Boundary Conditions

The NIST analyses with FDS show that the thermal gradients created by the fire would result in significant air flow past a body located in the tunnel downstream of the fire. This fire-forced convection would significantly affect heat transfer around the LWT cask or ISO container, and have a strong influence on the rate of increase of the outermost surface temperatures of the package. The regional peak gas temperatures shown in Figure 6.2 and associated velocities shown in Figure 6.3 were used to define local time-dependent Nusselt number values on the surface nodes corresponding to the upper, middle and lower regions of the package. The corresponding heat transfer coefficient is used to calculate the local convection heat at the package surface.

To maintain consistency between the two models, the same Nusselt number correlation was used to define convection heat transfer at the cask surface (without the ISO) as for the analysis of the package within an ISO container. For both cases, the Nusselt number at the outer surface of the package was defined using the following relationships for gas flow over flat or slightly curved surfaces at zero angle of attack [10];

for laminar flow ($Re_L < 500{,}000$):

$$Nu_L = 0.665\,Re_L^{1/2}\,Pr^{1/3}$$

for turbulent flow ($Re_L > 500{,}000$):

$$Nu_L = 0.032\,Re_L^{0.8}\,Pr^{1/3}$$

With the ISO container, the characteristic length, L, used in the ANSYS model to define the Nusselt number and Reynolds number for this application was the horizontal ISO container wetted surface length (i.e., 240 inches). For the case without the ISO container, the axial characteristic length was defined as 232 inches, based on the length of the exposed package body. A characteristic length of 65 inches was used for the vertical surfaces of the impact limiters on the ends of the cask.

The peak gas temperature predictions from the NIST analysis define the ambient sink temperatures around the package during the fire transient and post-fire cool down period. The Nusselt number defines the rate of heat transfer from the package, which is used in ANSYS to calculate the local convection heat flux at the outer surfaces. Using the one of the above relationships for Nusselt number (depending on the geometry being modeled and the hydrodynamics of the air flow), the code solves for local surface temperatures, T_s, and calculates the convection component of the heat flux at the surface using the formula

$$q''_{conv} = Nu_L \frac{k}{L}(T_s - T_{air})$$

where k = thermal conductivity of ambient air
L = characteristic length
T_s = cask surface temperature
T_{air} = ambient external air temperature.

Separate boundary types were defined for the top, sides, and bottom surfaces of the package using the external air temperatures shown in Figure 6.2. The velocities in Figure 6.3 were used to define the Nusselt number so that the boundary conditions on the cask would change with time.

By the end of 3 hours, the gas velocities predicted in the NIST calculation are down to 1 to 2 ft/s (0.3 to 0.6 m/s) or less (see Figure 3.15). Heat transfer at the package surface for these flow conditions is a complex mixture of forced convection (due to air flow induced in the tunnel by the temperature gradients of the fire) and free convection (driven by the non-uniform circumferential temperatures around the package outer surface).

At velocities below about 3-5 ft/s (1 to 1.5 m/s), heat transfer rates predicted assuming forced convection are generally lower than heat transfer rates due to natural convection for the temperatures on and around the surface of the package. To avoid the modeling uncertainties associated with mixed-mode heat transfer, forced convection only was assumed until the end of the NIST simulation, at 3 hours into the transient. From 3 hours to 50 hours, the heat transfer was assumed to be natural convection only. The contribution of free convection at the package surface is ignored in the cool down from 0.7 to 3 hours, and the contribution of forced convection is neglected in the cool down period from 3 to 50 hours. This ensures a conservative treatment of convection heat transfer from the package surface during the entire calculation.

For consistency, the natural or buoyancy-driven convective coefficients were those utilized to determine the pre-fire component temperature distributions (i.e., Normal-Hot Conditions of Transport, as defined in 10 CFR 71.71[1].) The heat transfer coefficients were defined for the appropriate surface geometries using the following relationships [11,12,13]:

--for flow along a vertical plane or cylinder:

--laminar flow ($10^4 < Gr_f \cdot Pr_f < 10^9$)

$$h = 1.42\left(\frac{\Delta T}{L}\right)^{1/4}$$

--turbulent flow ($Gr_f \cdot Pr_f > 10^9$)

$$h = 1.31(\Delta T)^{1/3}$$

where

h = heat transfer coefficient, W/m^2-°C
$\Delta T = T_w - T_\infty$, °C
T_w = surface or wall temperature, °C
T_∞ = ambient temperature, °C
L = vertical or horizontal dimension, *m*
Gr_f = Grashoff number of the gas at film temperature; $T_f = (T_w + T_\infty)/2$
Pr_f = Prandtl number of the gas at film temperature

--for flow over a horizontal cylinder:

--laminar flow ($10^4 < Gr_f \cdot Pr_f < 10^9$),

$$h = 1.32\left(\frac{\Delta T}{d}\right)^{1/4}$$

where

d = diameter, m

--turbulent flow ($Gr_f \cdot Pr_f > 10^9$),

$$h = 1.24(\Delta T)^{1/3}$$

--for flow over a horizontal heated plate facing upward (cool side facing downward):

-- laminar flow ($10^4 < Gr_f \cdot Pr_f < 10^9$),

$$h = 1.32\left(\frac{\Delta T}{L}\right)^{1/4}$$

-- turbulent flow ($Gr_f \cdot Pr_f > 10^9$),

$$h = 1.52(\Delta T)^{1/3}$$

--for laminar flow ($10^4 < Gr_f \cdot Pr_f < 10^9$) over a heated plate facing downward (cool side up):

$$h = 0.59\left(\frac{\Delta T}{L}\right)^{1/4}$$

Definitions of material properties used to compute $Gr_f \cdot Pr_f$ for use with these correlations were taken from Table A-3 of Kreith [13].

An empirical relationship for effective conductivity incorporating the effects of both conduction and convection was used to determine heat exchange through the liquid neutron shield. In the SAR [7] analysis for the LWT cask, the effective conductivity of the ethylene glycol mixture for conditions below 350°F was determined using the correlation of Bucholz [14]. This correlation defines the ratio of the effective conductivity to the actual thermal conductivity as equal to the Nusselt number, such that

$$\frac{k_{eff}}{k_c} = Nu = 0.135(Pr^2\, Gr/(1.36 + Pr))^{0.278}$$

where k_{eff} = effective thermal conductivity of material in node
k_c = thermal conductivity of motionless fluid in node
Pr = Prandtl number
Gr = Grashoff number.

The tunnel fire transient is outside the range of applicability of the Bucholz correlation, and it yields unrealistically large values for k_{eff} for these conditions. An alternative correlation from Raithby and Hollands [10], based on heat transfer between concentric cylinders, was used in this analysis instead. This correlation produces reasonable values of k_{eff}, and the transient conditions are generally within its applicable range. In this correlation, the Nusselt number is expressed as

$$\frac{k_{eff}}{k_c} = Nu = 0.386 D_r (Pr/(0.861 + Pr))^{0.25} Ra^{0.25}$$

where Rayleigh number (Ra = Pr*Gr) is based on the temperature difference across the annular gap.

The dimensionless parameter D_r is defined:

$$D_r = \left[\frac{\ln(D_o / D_i)}{d^{3/4}(1/D_i^{3/5} + 1/D_o^{3/5})^{5/4}} \right]$$

where D_o = annulus outer diameter
D_i = annulus inner diameter
d = width of annulus.

Figure 6.6 shows a plot of the Nusselt number predicted with these two correlations for the liquid (56% ethylene glycol and water mixture) in the neutron shield annulus.

Figures 6.7 and 6.8 show the effective conductivity for the annulus as a function of the average temperature and temperature difference for the liquid neutron shield tank and expansion tank, respectively. (The sharp discontinuity in the curves on both plots represents the abrupt phase change assumed when the average temperature of the liquid reaches the boiling point of the ethylene glycol and water mixture.) For low values of the temperature difference, the results approach those for conduction-only conditions.

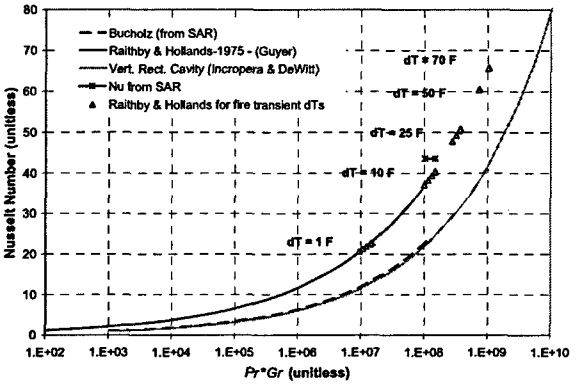

Figure 6.6. Nusselt Number for Heat Transfer in Liquid Neutron Shield

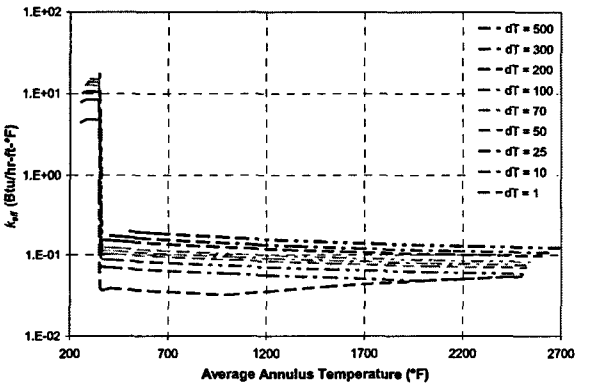

Figure 6.7. Effective Conductivity of Liquid Neutron Shield Tank

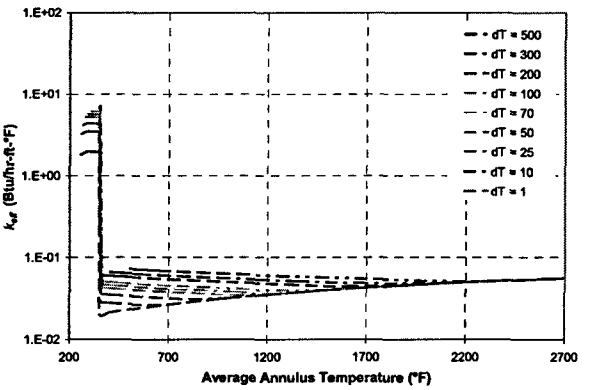

Figure 6.8. Effective Conductivity of Liquid Neutron Shield Expansion Tank

6.3 Initial System Component Temperatures

The hot normal conditions for transport were used as initial conditions for these analyses. A heat generation rate equivalent to a decay heat load of 8,530 Btu/hr (2.5 kW) was applied, with appropriate peaking factor, over the active fuel region. For the analysis of the cask without an ISO container, free convection at the package surface is handled by SURF152 elements with a constant heat transfer coefficient of 0.891 Btu/h-ft^2-°F (0.157 W/m^2-°C) and an ambient temperature of 100°F (38°C). For the analysis with the ISO container, the natural convection correlations for buoyancy-driven flow discussed in Section 6.2.2 were used to simulate convection heat transfer between the outer surface of the cask and the inner surface of the ISO container, and between the outer surface of the ISO container and ambient air.

For both analyses, with and without the ISO container, solar insolation (i.e., radiation) is incorporated by using SURF152 elements with heat generation on the outer surface of the package, at the rate specified in 10CFR71 [1]. For pre-fire conditions, the emissivity of the cask surface or ISO container surface was specified at a value representative of the local surface finish (e.g., 0.3 for bare stainless steel, 0.85 for painted surfaces.)

The steady-state temperature distributions predicted in the cask to define the initial conditions for the fire transient calculations were verified by comparison with results reported in the SAR [7]. Direct comparison is not possible, because the SAR [7] does not include any analytical cases similar to the detailed 3-D models used in this study. Because the main concern in analyses for normal transport conditions is to determine a conservative rate of heat removal from the cask, the applicant chose to perform a series of highly conservative evaluations using relatively simple models to qualify the system for its Certificate of Compliance (CoC).

The most complex models presented in the SAR [7] involve simple 2-D ANSYS cross-sections in which the cutting plane includes the expansion tank as well as the neutron shield tank. This approach does not allow axial heat flow out of the plane of the 2-D cross-section, and also assumes that the decay heat load axial peak occurs on that plane. This assumption places the spent nuclear fuel peak decay heat location under two concentric tanks filled with neutron shield material. This provides conservatism for a steady-state analysis, since the expansion tank makes a longer conduction path over which to dissipate the decay heat. For the fire transient, however, the assumptions in this 2-D model would limit the heat input to the cask from the fire, and would not constitute a conservative approach.

In the SAR [7], ANSYS cross-sectional models were also used to represent a 25-rod BWR basket assembly at 1.41 kW and a high burn-up PWR assembly at 2.1 kW. These models included detailed representation of the fuel pins, pin tubes, and can weldments with the pins resting on the pin tubes via point contact. These models also included the ISO container, with solar insolation and 100°F (38°C) ambient temperature.

The design basis results presented in Amendment 34 of the SAR [7] for a 2.5 kW PWR assembly also used a 2-D model of the cask. This is a HEATING5 model, with a 2-D axisymmetric representation using effective diameters for the basket and fuel assembly. This model neglects the ISO container and impact limiters, and the 2-D model cannot account for conduction and convection at the assembly end cavities. The ambient temperature boundary condition for these analyses was specified as 130°F (54°C).

The results reported for these three cases are summarized in Table 6.1. As might be expected, the conservative 2-D ANSYS models predict relatively high temperatures, compared to the results obtained with the more detailed HEATING5 model. Of these three cases, only the HEATING5 analysis at 2.5 kW is sufficiently close to the initial steady state conditions assumed for the fire transient to allow reasonable comparisons to be made for verification of the 3-D ANSYS model predictions.

Table 6.1. NAC LWT Component Temperatures at Various Decay Heat Loads

Component	2.5 kW °F (°C) (Table 3.4-2 [7])	1.41 kW °F (°C) Table 3.4-7 [7])	2.1 kW °F (°C) Table 3.4-10 [7])
Fuel Cladding	472 (244)	358 (181)	671 (355)
Aluminum PWR Insert	276 (136)	*	394 (201)
Inner Shell	274 (134)	249 (121)	385 (196)
Gamma Shield	273 (134)	248 (120)	375 (191)
Outer Cask Surface	229 (109)	185 (85)	308 (153)
Neutron Shield	238 (114)	235 (113)	306 (152)
Lid Seal	227 (108)	*	*
Drain/Vent Ports	231 (111)	*	*
Impact Limiters	*	*	*
ISO Container	*	*	*
* value not reported by applicant			

For the purpose of this comparison, additional calculations were performed with the 3-D ANSYS model, with and without an ISO container, using an ambient temperature boundary of 130°F (54°C) at 2.5 kW decay heat load. (These calculations were performed in addition to the cases at 100°F (38°C) ambient temperature, which provided the initial conditions for the fire transient calculation.)

Figure 6.9 shows the predicted temperature distribution from the ANSYS solution for this case with the cask in an ISO container. Table 6.2 presents detailed component temperature results obtained with the 3-D ANSYS model analyses, compared to the values published in the SAR [7] for the HEATING5 model at this decay heat load and ambient temperature boundary condition.

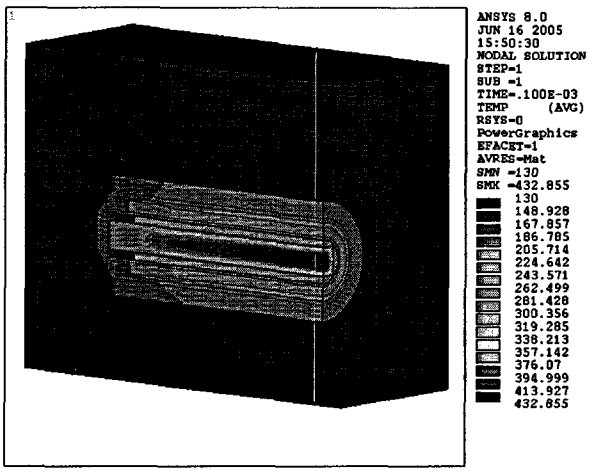

Figure 6.9. LWT Cask (with ISO Container): Normal-Hot Condition Temperature Distribution (2.5 kW Decay Heat, 130°F Ambient)

At first glance, the temperatures presented in Table 6.2 appear to show rather large differences between the results obtained with the two models. The peak clad temperature predicted with the ANSYS 3-D model is 434°F (223°C), compared to 472°F (244°C) reported in the SAR for the HEATING5 model [7]. Other component temperatures shown in the table are also lower for the 3-D ANSYS model results, compared to the corresponding SAR values. However, this is an expected result, given the modeling differences between the two cases. The 2-D cross-section representing the cask in the HEATING5 model should result in more conservative predicted temperatures, compared to the 3-D ANSYS model.

A more significant observation for the purposes of this comparison is that the differences in peak component temperature between the two approaches are consistent. The radial temperature drop from the peak fuel cladding temperature to the outer cask surface temperature is 234°F (130°C) for the ANSYS 3-D model, compared to

the predicted temperature drop of 243°F (135°C) with the HEATING5 axisymmetric model. This close agreement strongly suggests that both models provide a similar representation of the radial heat transfer paths from the fuel cladding to the environment. The differences in specific temperature values predicted are due mainly to differences in model complexity. The 3-D representation in the ANSYS model accounts for axial as well as radial heat transfer paths, which the 2-D HEATING5 model specifically excludes.

Table 6.2. NAC LWT Component Temperatures at 2.5 kW Decay Heat Load and 130°F Ambient

Component	Current Study, with ISO (ANSYS) °F (°C)	SAR Values (Table 3.4-2 [7]) °F (°C)	ΔT °F (°C)
Fuel Cladding	434 (223)	472 (244)	38 (21)
Aluminum PWR Insert	265 (129)	276 (136)	11 (6)
Inner Shell	228 (109)	274 (134)	46 (26)
Gamma Shield	227 (108)	273 (134)	46 (26)
Outer Cask Surface	200 (93)	229 (109)	29 (16)
Neutron Shield	204 (96)	238 (114)	34 (19)
Lid Seal	164 (73)	227 (108)	63 (35)
Drain/Vent Ports	164 (73)	231 (111)	67 (37)
Impact Limiters	167 (75)	Not Modeled	--
ISO Container	167 (75)	Not Modeled	--

Figure 6.10 shows the temperature distribution for the NAC LWT package within an ISO container, predicted with the ANSYS 3-D model for the initial steady-state conditions before the fire transient. Figure 6.11 shows the temperature distribution predicted for the NAC LWT package without an ISO container. The boundary conditions for these calculations were specified as 100°F (38°C) at 2.5 kW with solar isolation, corresponding to Normal Hot Conditions of Transport as described in 10 CFR 71.71 [1].

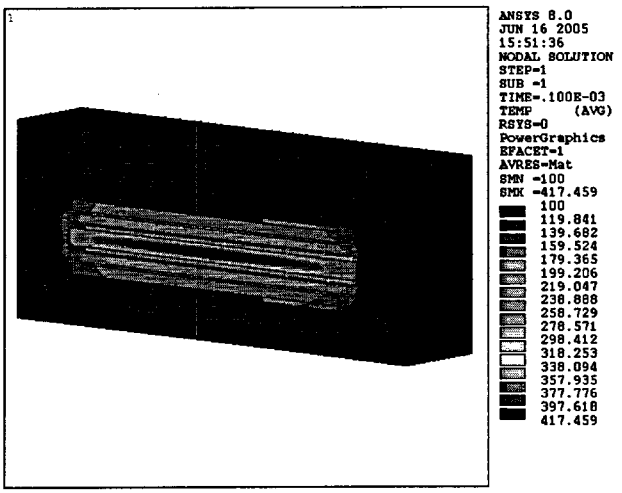

Figure 6.10. LWT Cask (with ISO Container): Normal Condition Temperature Distribution (2.5 kW Decay Heat)

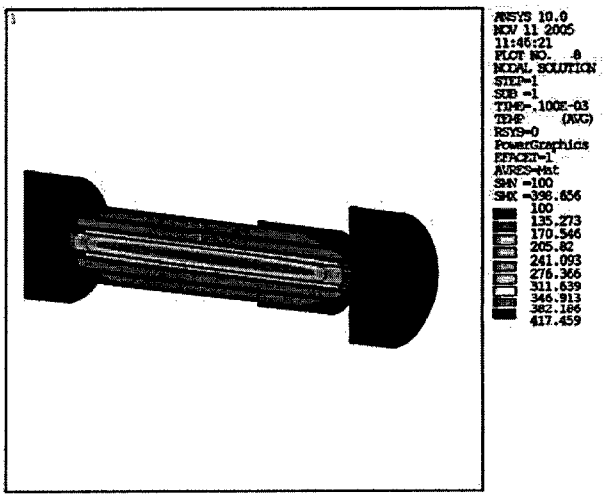

Figure 6.11. LWT Cask (without ISO Container): Normal Condition Temperature Distribution (2.5 kW Decay Heat)

The pre-fire steady-state component peak temperatures predicted with the ANSYS 3-D

models are shown in Table 6.3. These temperatures are somewhat lower than those reported for the 3-D model in Table 6.2, due to the lower ambient boundary temperature, but the temperature distribution is essentially identical.

Table 6.3. NAC LWT Pre-Fire Component Temperatures at 2.5 kW Decay Heat Load and 100°F Ambient

Component	without ISO (ANSYS) °F (°C)	with ISO (ANSYS) °F (°C)
Fuel Cladding	399 (204)	418 (214)
Aluminum PWR Insert	212 (100)	242 (117)
Inner Shell	172 (78)	205 (96)
Gamma Shield	171 (77)	204 (95)
Outer Cask Surface	138 (59)	176 (80)
Neutron Shield	144 (62)	180 (82)
Lid Seal	121 (49)	138 (59)
Drain/Vent Ports	120 (49)	138 (59)
Impact Limiters	122 (50)	141 (61)
ISO Container	N/A	140 (60)

6.4 Tunnel Fire Transient

The Caldecott Tunnel fire transient simulation for the NAC LWT transport package consists of three phases. The transient calculation is initiated from the steady-state conditions described in Section 6.3 (with or without the ISO container) for normal hot conditions, assuming insolation and 100°F (38°C) ambient temperature, as per 10CFR71.71 [1]. The first phase of the transient consists of the intense, gasoline-fueled fire, lasting approximately 40 minutes. The second phase consists of the short-term post-fire cool down, extending from the end of the fire (at 40 minutes) out the end of the NIST simulation with FDS, at 3 hours. The third phase consists of the long-term post-fire cool down, using extrapolated boundary conditions and extending from 3 hours out to 50 hours.

In the first phase of the calculation, the fire transient was initiated from the steady-state conditions by setting the solar insolation to zero, adding the elements and appropriate thermal connections comprising the model of the tunnel, and introducing the boundary conditions representing the fire. The transport package and tunnel surfaces were assign emissivities of 0.9 and 1.0, respectively, to represent surfaces affected by sooting.

For the first phase of the transient ($0 \leq t \leq 0.7$ hr), during the intense, gasoline-fueled fire, a forced convection regime was assumed to exist on the exterior of the package, with the surface heat transfer coefficient calculated based on the gas velocity predictions from the FDS analysis performed by NIST. With the gas temperatures from the NIST analysis defining the ambient boundary temperature, the convective heat flux at the package surface could be determined in the solution for the local surface temperature. Heat transfer due to thermal radiation was also included, with the source temperature for radiation exchange defined as the maximum of the tunnel wall temperature or tunnel gas temperature, to conservatively take into account the effects of optical densification due to smoke and other gasses released as a result of the fire.

As an additional conservatism to maximize the heat input to the package from the fire, the aluminum honeycomb impact limiters were assumed to remain intact during the fire. The heat conduction paths into the cask provided by the impact limiters were therefore maintained at the higher value corresponding to the aluminum honeycomb long after the predicted temperatures indicated that this material would have been destroyed or degraded by the fire. At the end of

the fire, the properties of the nodes representing this material were replaced with thermal properties of hot dry air.

Similarly, the ethylene glycol and water mixture in the neutron shield tanks was assumed to remain in place until the average temperature of this region exceeded the boiling temperature of the liquid (350°F (177°C)). At that point, it was assumed that the liquid was replaced by hot dry air.

In the second phase of the analysis, the post-fire cool down from the end of the fire (at 40 minutes) to the end of the FDS simulation (at 3 hours), the convective heat transfer at the package surface was assumed to consist of only forced convection, based on predicted gas velocities and temperatures from the NIST analysis with FDS. In the third phase of the analysis, the post-fire cool-down was extended from 3 hours out to 50 hours (49.3 hours after the end of the fire.) The boundary conditions for the additional 47 hours of the transient were obtained from the temperatures and velocities predicted in the FDS analysis, extrapolated to 50 hours using a power function (as discussed in Section 6.1.) In this phase of the transient, the boundary condition at the package surface was switched from forced convection to free convection.

Results obtained using the ANSYS models of the NAC LWT cask (with and without an ISO container) are discussed in Section 7.

7 ANALYSIS RESULTS

Due to temperature limits for the spent fuel cladding, closure seals, impact limiter materials, and neutron shield materials, these components are the most important elements to consider in evaluating the response of the transport systems to the fire scenario. The peak clad temperature limit is important because the cladding is the primary fission product containment boundary for the spent fuel. The temperature limit for the closure seals is important because these seals constitute the outer-most containment boundary for the cask. The temperature limits for the neutron shield material and impact limiters are important because these materials are generally the most vulnerable to damage or destruction during the fire. The results of the analyses of the NAC LWT package are evaluated primarily in relation to the peak predicted temperatures for these components in the fire transient.

The ANSYS model of the NAC LWT package consists of 52,446 standard computational elements and 16 superelements that are solved each time step. Calculations with this model yield detailed temperature distributions that can be analyzed to characterize the cask response to the specified boundary conditions. The system response predicted for the NAC LWT package with ANSYS for the fire transient conditions is presented in the following three subsections, for the three phases of the transient, as outlined in Section 6.4.

Section 7.1 presents the predicted response for the first phase, which consists of the intense gasoline-fueled fire (i.e., the first 40 minutes of the transient.) Section 7.2 presents results for the second phase of the transient, which consists of the short-term post-fire cool down. This phase extends from the end of the fire (at 40 minutes) to the end of the NIST simulation with FDS (at 3 hours.) Section 7.3 presents results for the third phase of the transient, which consists of the long-term post-fire cool down from 3 hours out to 50 hours, using boundary conditions extrapolated from the cool down portion of the FDS simulation.

7.1 NAC LWT Package Response to Fire Transient

Figure 7.1 shows the temperature response for the NAC LWT cask and ISO container predicted with ANSYS for the first hour of the transient. Figure 7.2 shows the temperature response for the NAC LWT cask without an ISO container for the same boundary conditions. This time interval encompasses the intense gasoline-fueled fire, which lasted approximately 40 minutes, plus the first 20 minutes of the post-fire cool down period.

For both cases, the temperature response is very nearly identical during this time interval. Without the ISO container, temperatures of outboard components (i.e., cask surface, vent/port seals, and impact limiters) rise somewhat faster and reach slightly higher peak temperatures during the fire. However, the differences are relatively small, and in both cases, the cask package exhibits essentially the same response to the fire. In both cases, most components reach their peak temperature values during this interval, closely following the high boundary temperatures during the fire and their rapid decrease once the gasoline is consumed.

This behavior is due to the relatively low thermal inertia of the package, because of its relatively small physical size. Direct conduction paths into the cask are relatively short, and its surface-to-volume ratio is relatively large.

Without the ISO container, thermal radiation heat transfer views include a large portion of the cask surface, due to the horizontal orientation of the package within the tunnel. Similarly, the surfaces of the ISO container have essentially one-to-one views of the tunnel ceiling, walls, and floor.

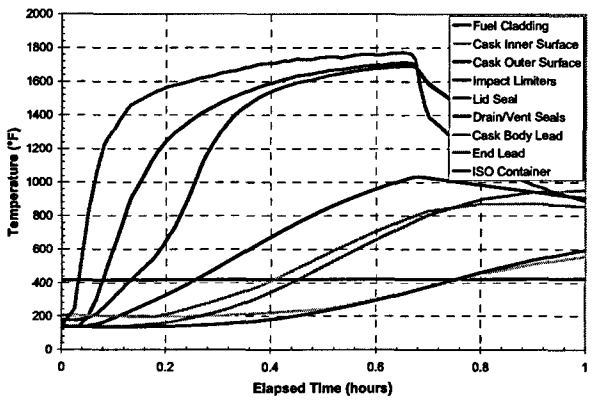

Figure 7.1. NAC LWT Cask (with ISO Container): Component Maximum Temperature Histories During Fire Transient

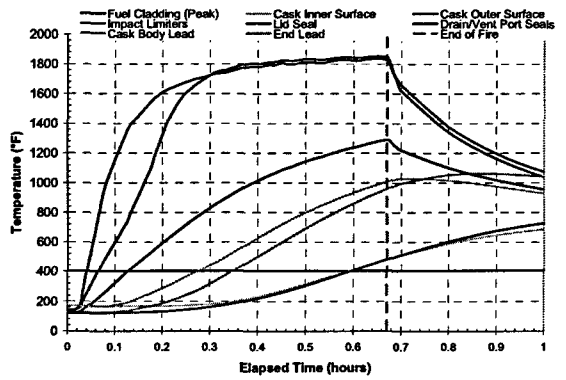

Figure 7.2. NAC LWT Cask (without ISO Container): Component Maximum Temperature Histories During Fire Transient

Without the ISO container, the maximum temperature on the exterior surface of the cask reaches a peak value of 1853°F (1012°C) at 0.65 hr, just before the end of the fire. For the case with the ISO container, the maximum temperature on the exterior surface of the cask is only 1694°F (923°C), reached at 0.67 hr. This is because the ISO container acts as a thin thermal shield, protecting the cask surface from the direct radiation view of the fire. The ISO container itself reaches a peak temperature of 1773°F (967°C) at about 0.67 hr. This value is higher than the peak temperature on the cask surface for this simulation, but is still somewhat lower than the peak temperature on the unshielded cask, in the case without the ISO container.

These results show that the ISO container acts as a heat shield for the cask during the intense high-temperature portion of the fire, lowering the peak temperature on the cask surface by about 159°F (88°C). Similarly, the maximum temperature on the impact limiters is about 1837°F (1003°C) without the ISO container, compared to 1714°F (934°C) obtained with the ISO container, a difference of about 123°F (68°C). This effect is also seen in the maximum temperature for the drain and vent port seals. Without the ISO container, the nodes representing this component reach a peak value of 1287°F (697°C) by the end of the simulated fire, compared to 1035°F (557°C) in the case with the ISO container.

For both cases, with and without the ISO container, the peak temperatures of the cask inner shell material, lid seal, and the lead gamma shielding layers show a more gradual increase during the fire, and the temperatures of these components continue to rise after the end of the fire. At the end of the first hour of the transient, the peak temperature predicted for the cask inner surface has reached approximately 400°F (204°C) for the case with the ISO container, and is at about 685°F (363°C) for the case without the ISO container. In both cases, this

temperature is still rising at the end of the first hour of the transient, which is approximately 20 minutes after the end of the gasoline-fueled fire.

For the cask within the ISO container, the temperature of the lead layer within the cask body is predicted to reach a maximum of 870°F (466°C) at 0.9 hr elapsed time (i.e., about 15 minutes after the end of the simulated fire.) Without the ISO container, this temperature peaks somewhat earlier, just after the end of the fire at 0.7 hr, at the somewhat higher temperature of 1031°F (555°C). Similarly, the temperature of the lead layer in the cask bottom is predicted to reach a maximum of 952°F (511°C) at 1 hr elapsed time for the cask within the ISO container, while the peak is 1061°F (572°C) for this component in the case with no ISO container.

For both cases, these peak temperatures in the lead shielding are considerably above the established operating limit of 600°F (316°C) reported in the SAR [7] for this material. This suggests that there could be melting and slumping of the lead as a result of the fire. However, for the purposes of the thermal analysis, the lead is assumed to remain intact, to preserve the good conduction path through the material and conservatively maximize heat input to the cask during the transient. Also, as a further conservatism, the energy that would be absorbed by the material phase change in the process of melting the lead is not subtracted from the thermal load imposed on the cask by the fire.

Because of the relatively low boiling point of the ethylene glycol solution in the neutron shield tank and overflow tank, the liquid is expected to boil off as part of the cask response to the fire transient, with or without the ISO container. As described in Section 5, the predicted temperatures in the main tank and overflow tank were monitored throughout the transient solution to determine the predicted time of rupture and evaporation. Consistent with the standard fire analysis included in the SAR [7], the tanks were assumed to rupture when the predicted temperature exceeds the ethylene glycol boiling point of 350°F (177°C). As an additional measure of conservatism, to further maximize the heat input to the cask during the fire, tank rupture was assumed to occur only after the average ethylene glycol temperature exceeded 350°F (177°C), rather than at the point when the peak temperature reached this value.

Using this criterion, the ANSYS analysis for the case with the ISO container predicts that the outer expansion tank would rupture at approximately 13 minutes into the fire, and the inner tank would rupture at about 18 minutes. For the case without the ISO container, this transition occurs slightly earlier, at about 10.5 minutes for the outer tank and 13 minutes for the inner tank.

In both cases, basing the times of rupture for the two tanks on the average temperature rather than the peak temperature delays rupture to a slightly later point in the transient than would be predicted based on the peak temperature. The effect of this assumption is to increase the heat input into the cask due to the fire, by extending the time interval that the relatively high conductivity ethylene glycol remains in the tanks. Following rupture, the effective conductivity of the expansion tank decreases significantly as a result of the expulsion of the ethylene glycol volume, which is assumed to be replaced with air. Cooling effects associated with this boiling process are neglected in the heat transfer solution. However, the calculation fully accounts for thermal radiation between the hot walls of the empty tanks.

The temperature response of the fuel cladding is the slowest of all components in the cask, due to the significant thermal inertia of the fuel, and because it has the longest heat transfer path to the fire. For the case with the ISO container, the predicted peak fuel cladding temperature has increased by only about 5°F (2.8°C), at the end of the gasoline-fueled fire. For the case without the ISO container, the increase is slightly smaller, only about 3.7°F (2°C). However, in both cases, the rod surface temperatures are increasing along the entire length of the assembly, as a result of the ends of the fuel assembly being exposed within the open cavities at the top and bottom of the cask. This is illustrated in Figure 7.3 for the calculation with the ISO container. (The results for the calculation without the ISO container are virtually indistinguishable at this point in the transient, and therefore are not shown in a separate plot.)

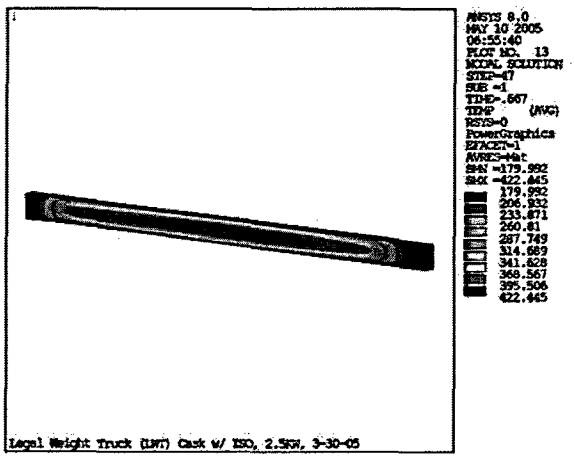

Figure 7.3. Lumped Fuel Assembly Temperature Distribution 0.7 hr into Transient

In both cases, the ends of the fuel rods directly see the inner shell and ends of the cask. As the inner shell surrounding these ends heats up, thermal radiation exchange within the cavities transfers heat directly to the rod array. For this portion of the transient (i.e., during the simulated fire) the peak fuel temperature occurs at the center of the assembly (see Figure 7.3).

7.2 NAC LWT Package Short-Term Post-Fire Transient Response

Figure 7.4 shows the peak temperatures predicted for components of the cask within the ISO container during the first three hours of the ANSYS transient simulation. Figure 7.5 shows the peak temperatures for these components predicted for the cask without the ISO container. In both cases, the cladding peak and average temperatures continue to rise after the simulated fire, due to the severe temperature environment in the tunnel. The ambient conditions in the tunnel immediately following the simulated fire significantly retard the rate at which the fuel decay heat can be removed from the cask.

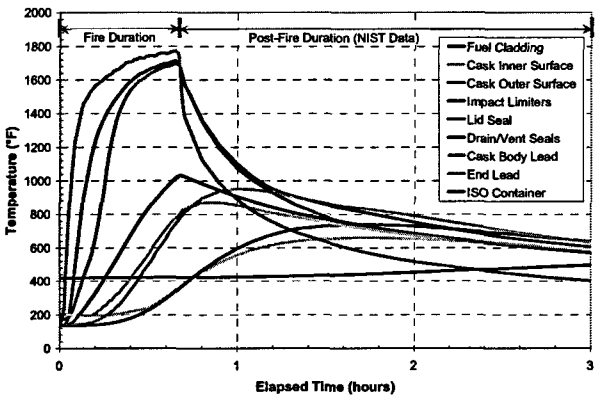

Figure 7.4. NAC LWT Cask (with ISO Container): Maximum Temperature Histories for First 3 hours of Fire Transient

Once the simulated fire is over, however, the predicted peak temperatures on outboard components begin to drop rapidly. As noted in Section 7.1 for the calculations with and without

the ISO container, the cask outer surface, the impact limiters, and drain and vent port seals reach their peak temperatures by the end of the simulated fire, and the lead gamma shielding components reach their peak temperatures within the first hour of the transient. The peak temperatures on the cask inner surface and the lid seal reach their respective maximum values at a slightly later time; approximately 1.7 hrs into the transient for the case with the ISO container, and at about 1.3 hrs in the case without the ISO container.

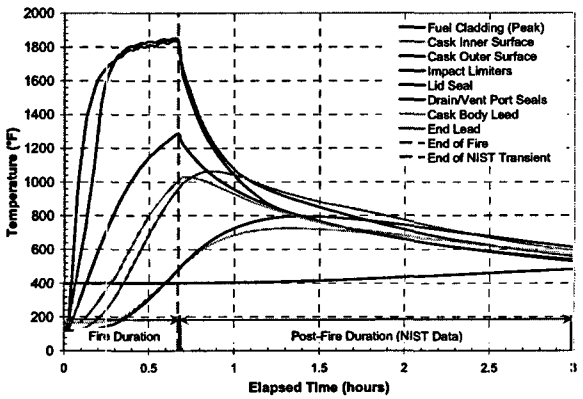

Figure 7.5. NAC LWT Cask (without ISO Container): Maximum Temperature Histories for First 3 hours of Fire Transient

This behavior is in response to the rapidly decreasing boundary temperatures, as illustrated by the ISO container peak temperature in Figure 7.6, and the cask peak surface temperature (for the case without the ISO container) in Figure 7.7. These figures compare the predicted peak temperature of the ISO container or the cask outer surface to the boundary temperatures for the tunnel ceiling and upper tunnel air from the NIST calculation with FDS.

Figures 7.4 and 7.5 show that in both cases (with and without the ISO container) the peak temperatures for all cask components except the fuel begin to decrease at or shortly after the end of the fire. As a result of the low thermal inertial of this cask, peak temperatures in most components occur within about an hour after the end of the fire. The exception is the peak cladding temperature, which responds much more slowly to the adverse heat transfer conditions imposed by the fire transient.

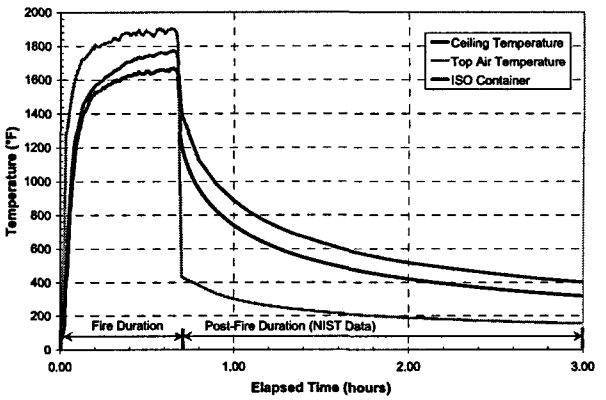

Figure 7.6. Maximum Predicted ISO Container Surface Temperature History Compared to NIST Boundary Condition Temperatures

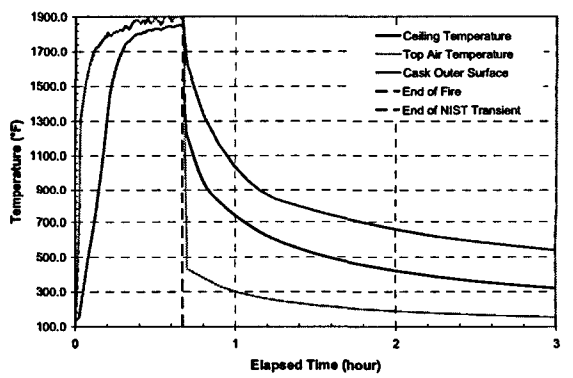

Figure 7.7. Maximum Predicted Cask Outer Surface Temperature History for NAC LWT Cask without ISO Container Compared to NIST Boundary Condition Temperatures

In both cases, the peak clad temperature is still rising after three hours. However, it is predicted to be only about 497°F (258°C) by this time, for the case with the ISO container. Without the ISO container, the peak clad temperature is predicted to be 482°F (250°C) by the end of three hours.

For the case with the cask within the ISO container, Figure 7.8 shows the maximum temperature histories predicted for the seals in the drain/vent ports and the lid for the first 3 hours of the transient. Figure 7.9 shows the maximum temperatures of these components for the case without the ISO container. (The calculated values were gathered by querying nodes at the seals' locations, since the seals were not explicitly represented in the model.) The drain and vent ports are sealed with TFE or Viton® O-rings. The bolted lid is sealed with metallic and TFE O-ring seals. For the cask within the ISO container, the drain and vent port seals are predicted to reach a maximum temperature of 1035°F (557°C) by the end of the simulated fire. Similarly, for the cask without an ISO container, these seals are predicted to reach a maximum temperature of 1287°F (697°C) by the end of the fire. The lid seal is predicted to reach 740°F (393°C) at 1.7 hr elapsed time for the cask within an ISO container. Without an ISO container, the lid seal is predicted to reach 795°F (424°C) at 1.33 hr elapsed time in the transient.

In both cases, the seal materials then gradually decrease in temperature as the transient proceeds into the post-fire cool down. The extreme rise in temperature during and immediately after the fire is due to the low thermal inertia of the NAC LWT cask and the close proximity of the seals to exterior surfaces subject to thermal radiation directly from the tunnel environment, or from the inner surface of the ISO container.

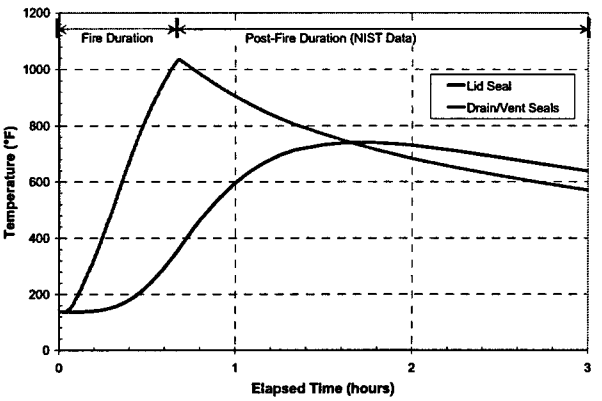

Figure 7.8. NAC LWT Cask (with ISO Container): Maximum Seal Temperature Histories for Drain/Vent Ports and Cask Lid During First 3 hours of Fire Transient

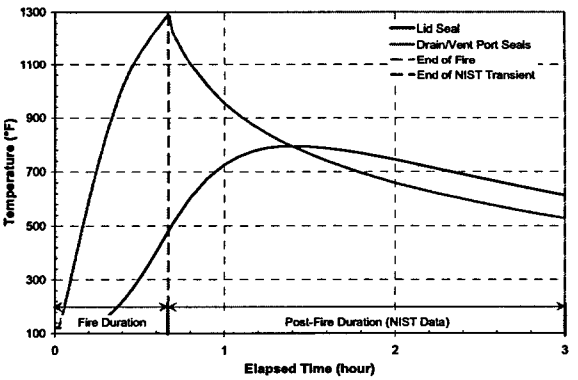

Figure 7.9. NAC LWT Cask (without ISO Container): Maximum Seal Temperature Histories for Drain/Vent Ports and Cask Lid During First 3 hours of Fire Transient

With or without an ISO container, the maximum seal temperatures predicted in this transient exceed the maximum continuous-use temperature limits of the drain and vent port seals used in this cask design. In the lid seal region, the predicted maximum temperature is 740°F (393°C) for the case with the cask in an

ISO container, and is 795°F (424°C) without an ISO container. Both are below the maximum continuous-use temperature limit of 800°F (427°C) for the metallic seals, but exceed the maximum continuous-use temperature limit of of the drain and vent port seals. These limits are 735°F (391°C) for TFE seals and 550°F (288°C) for the alternative design Viton® seal. For the drain and vent port seals, the predicted maximum temperature values in both cases (1035°F (557°C) with an ISO container, and 1287°F (697°C) without an ISO container), are several hundred degrees above the maximum continuous-use temperature limits for these seal materials.

Figures 7.8 and 7.9 show that in both cases, with and without an ISO container, the lid seal region maintains temperatures at or near the peak temperature values for a relatively short time before beginning a steady decrease. Similarly, the maximum temperature values predicted in each case for the drain and vent port region climbs very rapidly to the peak value, then steadily decreases. This component is above the maximum continuous-use temperature limit for less than two hours. Since the noted limits for the Viton®, TFE, and metallic O-ring materials are defined for continuous use, it is possible that the seals might survive these temperature excursions undamaged.

However, information is not available on the recommended short-term temperature limits for these seals. Based on the continuous-use temperature limits, the primary containment barrier of the NAC LWT is considered to degrade at the drain/vent ports and possibly at the lid seal under the postulated conditions of this fire transient, with or without an ISO container. An analysis evaluating the possible radiological consequences of the NAC LWT cask responses to the Caldecott Tunnel fire is presented in Section 8.

7.3 NAC LWT Package Long-Term Post-Fire Transient Response

To evaluate the effects of prolonged exposure to post-fire conditions in the tunnel, the temperatures predicted in the NIST analysis were extrapolated from 3 hours to 50 hours using a power function in order to realistically model the extended cool down of the tunnel environment. (See Section 6.2; the extrapolated values are presented in Figures 6.4 and 6.5 for the radiation and convection heat transfer boundary conditions, respectively.) This conservative approach is equivalent to assuming that the cask will be left in the tunnel up to two days without any emergency responder intervention.

The external boundary conditions were extended using the conservative assumption of a purely forced convection heat transfer regime for the first 3 hours of the simulation, then a purely free convection regime for the remainder of the calculation ($t \geq 3$ hours). Figure 7.10 shows the temperature response of various components of the cask for the long term transient calculation to 50 hours, with the cask enclosed in an ISO container. A similar plot is shown in Figure 7.11 for the case of the cask without an ISO container.

The maximum temperatures for most components were reached within a short time after the simulated fire, (see Sections 7.1 and 7.2.) However, the predicted maximum fuel cladding temperature of 558°F (292°C) for the cask within an ISO container is not reached until about 8 hours into the transient. Without an ISO container, the peak clad temperature is reached approximately one hour sooner, at 7 hours into the transient, and the maximum temperature is somewhat lower, at 539°F (282°C).

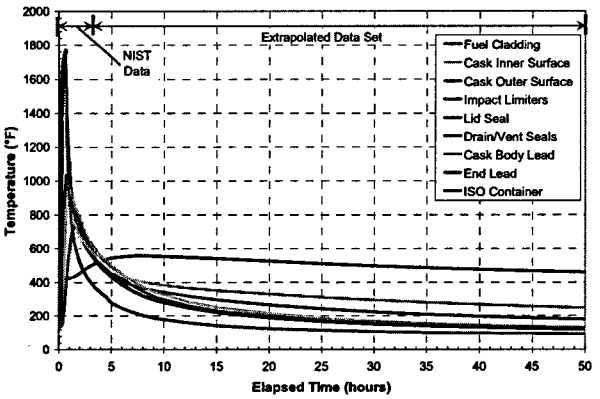

Figure 7.10. NAC LWT Cask (with ISO Container): Maximum Temperature Histories During 50 hour Transient

This difference is due to the effect of the ISO container on the rate of heat removal from the cask in the post-fire cool down. The ISO container shields the cask from the external environment, slowing the rate of heat input to the cask during the fire, and resulting in slightly lower peak temperatures on most of the cask components, compared to the values predicted without the ISO container. However, after the fire, the ISO container slows the rate of heat removal from the cask to the cooling tunnel environment. The unshielded cask, in the case without the ISO container, shows a slightly faster cool down, and does not reach as high a value for the maximum peak cladding temperature during the transient.

With or without the ISO container, the peak clad temperature does not exceed the long-term storage temperature limit of 752°F (400°C), and is far below the currently accepted short-term temperature limit[2] of 1058°F (570°C) for Zircaloy clad spent nuclear fuel under accident conditions [17].

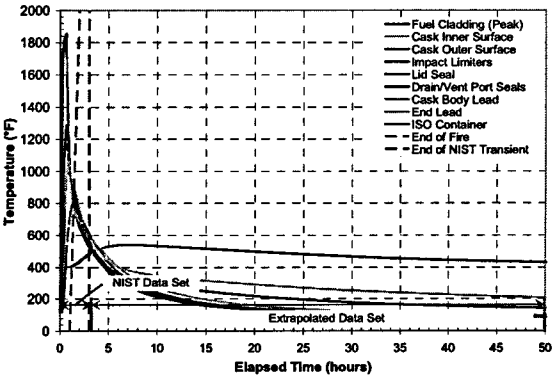

Figure 7.11. NAC LWT Cask (without ISO Container): Maximum Temperature Histories During 50 hour Transient

The plots in Figures 7.10 and 7.11 also show that the NAC LWT cask is very close to a new steady state for the extrapolated conditions in the tunnel at 50 hours. This behavior is consistent with the lower thermal inertia of this cask, compared to the expected response of larger multi-assembly casks to severe fire transient conditions. The temperature distributions within the cask predicted for these two cases (with and without the ISO container) for the final steady state differ somewhat from the temperatures predicted for the initial conditions at the start of the transient.

The differences are the result of the changes in the physical condition of the package after the fire, and the different boundary conditions for the post-fire ambient environment of the tunnel. As a result of the fire, the liquid neutron shield has boiled away, the cask outer surfaces (or the surfaces of the ISO container) have a much

[2] The short-term temperature limit of 1058°F (570°C) is based on creep experiments performed on two fuel cladding test samples which remained undamaged when held at 1058°F (570°C) for up to 30 and 71 days [15]. This is a relatively conservative limit, since the temperature at which Zircaloy fuel rods actually fail by burst rupture is approximately 1382°F (750°C)[16].

higher emissivity due to sooting, and the impact limiters have been damaged. In addition, the ambient temperatures in the tunnel are lower than those assumed for Hot-Normal conditions of transport, and there is no solar insolation.

7.4 Summary of NAC LWT Package Peak Temperatures in Fire Transient

Peak component temperatures over the entire transient fire simulation predicted for the NAC LWT cask (with and without the ISO container) are reported in Table 7.1. These results show that for both cases, the lead shielding within the cask body is expected to reach temperatures that far exceed the established safe operating limit of 600°F (316°C) [7] for this material. The predicted peak temperature of the lead shielding for the cask within the ISO container is 870°F (466°C) at 0.9 hr elapsed time, and the lead in the bottom end of the cask is predicted to reach a maximum temperatures 952°F (511°C) at 1 hr elapsed time.

For the cask without the ISO container, the peak temperatures in the lead shielding are slightly higher, and are reached at a slightly earlier time in the transient. The predicted peak temperature in the cask lead shielding is 1031°F (555°C), and the lead in the bottom end of the cask is predicted to reach a maximum temperatures 1061°F (572°C). In both cases, the lead remains fully contained within the steel cask body. However, melting and possible slumping of the shielding material within the steel containment is expected.

In the severe conditions of this fire scenario, the aluminum honeycomb material of the impact limiters mounted on the ends of the cask is expected to reach temperatures that are approximately 500-600°F (278-316°C) above its commonly estimated melting temperature. In the case without the ISO container, the predicted peak temperature on this component is approximately 123°F (68°C) hotter than in the case with the ISO container. Without the ISO container, the impact limiters are directly exposed to the intense heat of the fire, rather than being shielded by the walls of the container. In either case, however, the impact limiters cannot reasonably be expected to remain intact after the fire. However, these components are not part of the cask structure, and are generally expected to be damaged or destroyed by accident conditions. Their loss in the fire is not expected to adversely affect the thermal performance of the cask.

Table 7.1. NAC LWT Package Peak Component Temperatures During Fire Transient

Component	without ISO (ANSYS) °F (°C)	Time (hours)	with ISO (ANSYS) °F (°C)	Time (hours)
Fuel Cladding	539 (282)	7.00	558 (292)	8.00
Aluminum PWR Insert	425 (218)	4.50	444 (229)	5.00
Inner Shell	726 (386)	1.33	661 (349)	1.70
Lead Gamma Shield	1031 (555)	0.70	870 (466)	0.90
Lead End Shield	1061 (572)	0.90	952 (511)	1.00
Outer Shell	1853 (1012)	0.65	1694 (923)	0.67
Liquid Neutron Shield	1834 (902)	0.65	1656 (902)	0.65
Lid Seal	795 (424)	1.33	740 (393)	1.70
Drain/Vent Ports	1287 (697)	0.67	1035 (557)	0.68
Impact Limiters	1837 (1003)	0.65	1714 (934)	0.65
ISO Container	N/A		1773 (967)	0.65

8 POTENTIAL CONSEQUENCES

USNRC staff evaluated the potential for a release of radioactive material from the NAC LWT transportation cask analyzed for the Caldecott Tunnel fire scenario. The analysis indicates that the possibility of a release cannot be entirely ruled out for this cask because temperatures in the drain and vent port seal regions during the transient exceed the continuous-use temperature limit for the TFE or Viton® seals. Although the cask lid peak temperature remains significantly below the continuous-use temperature limit for its metallic seal, it exceeds the continuous-use temperature limit for its TFE seal.

Staff performed an analysis to determine the magnitude of any potential release. Based on that analysis (described below), it was determined that any potential release from the NAC LWT cask would be small—less than an A_2 quantity.[3] The potential release would not involve a release of spent fuel or fission products, but could possibly result from CRUD spalling off the fuel rods.

8.1 Release Analysis

The thermal analyses for the NAC LWT cask (with and without an ISO container) show that during the Caldecott Tunnel fire scenario this cask design would maintain the single most important barrier (i.e., the fuel cladding) to prevent the release of radioactive materials. The temperature of the fuel cladding is conservatively predicted to reach 558°F (292°C) when the cask is enclosed within an ISO container. The predicted peak cladding temperature is only 539°F (282°C) when it is assumed that the cask is not enclosed within an ISO container. These predicted peak temperatures are well below the long-term cladding temperature limit of 752°F (400°C) for normal storage and transport conditions. These peak temperatures are much lower than the cladding short-term temperature limit of 1058°F (570°C), and far below its projected burst temperature of 1382°F (750°C).

The maximum temperatures predicted for the TFE seals used in the NAC LWT cask lid and the drain and vent ports approach or exceed the rated continuous-use temperature limit of 735°F (391°C) for this material. The predicted temperatures also exceed the safe operating temperature of 550°F (288°C) for the alternative design Viton® seals for the drain and vent ports. The maximum temperature predicted for the lid is 740°F (393°C) for the cask within an ISO container, and 795°F (424°C) without an ISO container. The peak temperature of the vent and drain port seals is predicted to reach 1035°F (557°C) for the cask within an ISO container, and 1287°F (697°C) without an ISO container.

Exceeding the service temperature of the seals on the NAC LWT cask lid or vent and drain ports means that there is the potential for a release to occur. Potential releases from the drain and vent ports would be limited, however, by the narrow, convoluted flow paths of these structures. Potential releases through the lid seals would be limited by the presence of the undamaged metallic seal, and by the tight clearances of the close metal-to-metal contact between the lid and cask body. The close contact is maintained by the pre-load created by the initial torque on the lid bolts.

[3] An A_2 quantity represents the threshold below which an accident resistant package is not required. The acceptance requirement for Type B packages is that they release less than an A_2 quantity/week after being subjected to the hypothetical accident conditions in 10 CFR Part 71 [1].

Because the fuel cladding remains intact, it is not expected that any radioactive material would be released from inside the fuel rods. Any release of radioactive material from the cask would consist only of CRUD particles that may flake off or spall from individual fuel rods.

The amount of releasable CRUD in the NAC LWT cask was estimated using data developed by Sandia National Laboratory for analysis of CRUD contribution to shipping cask containment requirements [18], and assuming the cask contains a PWR fuel assembly consisting of 289 fuel rods. An estimate of the maximum "spot" CRUD activity shows that for 90% of PWR spent fuel rods the maximum activity is 20 μCi/cm^2 or less [18, Table I-15]. The ratio of the peak (i.e., the maximum "spot" CRUD activity) to average concentration on the rod surface varies by a factor of two for PWR fuel rods [18, Table I-12].

The CRUD activity estimates [18] are for newly discharged spent nuclear fuel. This activity is expected to decay by a factor of one-half for five-year cooled fuel, based on the decay rate for Co^{60}. This is a good approximation because 92% of the activity for five-year cooled fuel comes from Co^{60}. Based on this data, the average CRUD activity for five-year-cooled PWR fuel rods is about 0.006 curies per rod, based on a surface area of 1200 cm^2 per rod. The average CRUD activity for a 17 x 17 PWR assembly is therefore about 1.73 curies.

The amount of CRUD that could flake or spall from the surface of a PWR rod due to temperatures calculated for the fuel rods in the thermal analysis is estimated to be a maximum of 15% [18, Table I-10]. The major driving force for material release results from the increased gas pressure inside the cask due to increases in internal temperature. The temperature change in the cask is bounded by the difference between the maximum gas temperature predicted during the fire transient and the gas temperature at the time the cask is loaded. For this analysis, the loading temperature is defined as 100°F (38°C), based on the value reported in the SAR [7]. The maximum gas temperature is assumed to be the maximum peak clad temperature predicted during the transient. This yields a conservative estimate of the maximum possible temperature change.

A deposition factor of 0.90 was used to account for the deposition of CRUD particles on cask surfaces and fuel assemblies. This factor was developed as part of NRC security assessments for spent nuclear fuel transport and storage casks, and is based on an analysis of the gravitational settling of small particles. The value of 0.90 is conservative because it does not consider the effects of particle conglomeration and plugging. It is also consistent with the values used in other studies [16]. The major assumptions used to estimate CRUD release are given in Table 8.1.

Table 8.1. Assumptions Used for Release Estimate for NAC LWT Cask

Parameter	Assumed value
Number of Assemblies in Cask	1 PWR
Rods per Assembly	289
Maximum "spot" CRUD Activity on Fuel Rod	20μCi/cm^2
Peak to axial average variation	2
CRUD decay factor (5 yr) (based on Co^{60})	0.5
Average surface area per rod	1200 cm^2
Average CRUD Activity on PWR Fuel Rod (5 yr cooled)	0.006 Ci
Average CRUD Activity on PWR Assembly (5 yr cooled)	1.73 Ci
Fraction of CRUD released due to heating	0.15
Deposition Factor	0.90

To estimate the potential release from the NAC LWT cask, a methodology similar to that developed at Sandia National Laboratory (for NUREG-6672 [16]) was used. This methodology was developed for evaluation of the generic risks associated with the transport of spent fuel by truck and rail from commercial power plants to proposed interim storage and disposal sites.

The potential release from the cask in this severe fire accident can be calculated from the following relationship:

$$R = C_I S(1-D)\left(1-\frac{T_i}{T_p}\right)$$

where R = release (curies)
C_I = amount of CRUD on fuel assemblies (curies)
S = fraction of CRUD released due to heating
D = deposition factor
T_p = peak internal temperature (°R)
T_i = initial internal temperature (°R)

Table 8.2 shows the results obtained when this equation is applied using the parameter values from Table 8.1 and the temperatures predicted for the NAC LWT cask in this accident scenario. The analysis for the cask within an ISO container resulted in the higher predicted maximum peak clad temperature (558°F (292°C), compared to 539°F (282°C) without an ISO container), so this value was used in determining the potential release estimate.

Table 8.2. Potential Release Estimate for NAC LWT Cask

Initial temperature °F (°R)	Peak temperature °F (°R)	Potential release (curies)
100 (560)	558 (1018)	0.01

The potential release from the NAC LWT cask based on five-year cooled fuel is estimated to be approximately 0.01 curies of Co^{60}. Since the A_2 value for Co^{60} is 11 curies, the potential release is about 0.001 of an A_2 quantity (see footnote 2). Therefore, the potential radiological hazard associated with an accident similar to the Caldecott Tunnel fire, if it were to involve a spent nuclear fuel cask in close proximity to the fire source, is quite small. The probability of such an occurrence, based on tunnel accident frequency, flammable materials trucking accident statistics, and radioactive material shipment statistics, has been estimated as one such accident every million years [19].

9 REFERENCES

1. 10 CFR 71. Jan. 1, 2003. *Packaging and Transportation of Radioactive Material.* Code of Federal Regulations, U.S. Nuclear Regulatory Commission, Washington D.C.

2. NTSB/HAR-83/01. 1983. *Multiple Vehicle Collisions and Fire: Caldecott Tunnel, near Oakland, California, April 7, 1982.* National Transportation Safety Board, Bureau of Accident Investigation, Washington D.C.

3. McGrattan KB, HR Baum, RG Rehm, GP Forney, JE Floyd, and S Hostikka. November 2001. *Fire Dynamics Simulator (Version 2), User's Guide.* NISTIR 6784, National Institute of Standards and Technology, Gaithersburg, Maryland.

4. McGrattan KB. May 2005. *Numerical Simulation of the Caldecott Tunnel Fire, April 1982.* NISTIR 7231, National Institute of Standards and Technology, Gaithersburg, Maryland.

5. Bechtel/Parsons Brinkerhoff, Inc. November 1995. *Memorial Tunnel Fire Ventilation Test Program, Comprehensive Test Report,* Prepared for Massachusetts Highway Department and Federal Highway Administration.

6. McGrattan KB, HR Baum, RG Rehm, GP Forney, JE Floyd, and S Hostikka. November 2001. *Fire Dynamics Simulator (Version 2), Technical Reference Guide.* NISTIR 6783, National Institute of Standards and Technology, Gaithersburg, Maryland.

7. NRC Docket Number 71-9225. *Legal Weight Truck Transport (LWT) Packaging Safety Analysis Report,* July 2000, Rev. 2; September 2001, Rev. 33; Rev. 34. Nuclear Assurance Corporation, Atlanta, Georgia.

8. ANSYS, Inc. 2003. "ANSYS Users Guide for Revision 8.0," ANSYS, Inc., Canonsburg, Pennsylvania.[4]

9. Bahney RH III, TL Lotz. July 1996. *Spent Nuclear Fuel Effective Thermal Conductivity Report,* BBA000000-01717-5705-00010 Rev. 00. TRW Environmental Safety Systems, Inc., Fairfax, Virginia.

10. Guyer EC and DL Brownell, editors. 1989. *Handbook of Applied Thermal Design.* McGraw-Hill, Inc., New York, p. 1-42.

11. Kreith F and MS Bohn. 2001. *Principles of Heat Transfer, 6th Edition.* Brooks/Cole, Pacific Grove, California.

12. Holman JP. 1986. *Heat Transfer, 6th Edition.* McGraw-Hill, Inc.

13. Kreith F. 1976. *Principles of Heat Transfer, 3rd Edition.* Intext Education Publishers, New York.

14. Bucholz JA. January 1983. *Scoping Design Analyses for Optimized Shipping Casks Containing 1-, 2-, 3-, 5-, 7-, or 10-year old PWR Spent Fuel.* ORNL/CSD/TM-149. Oak Ridge National Laboratory, Oak Ridge, Tennessee.

15. Johnson AB and ER Gilbert. September 1983. *Technical Basis for Storage of Zircaloy-Clad*

[4] ANSYS Release 10.0 (2005) was used for some of the graphical post-processing, but all fire transient simulations of the NAC LWT package were performed with ANSYS Release 8.0.

Spent Fuel in Inert Gases, PNL-4835. Pacific Northwest Laboratory, Richland, Washington.

16. Sprung JL, DJ Ammerman, NL Breivik, RJ Dukart, and FL Kanipe. March 2000. *Reexamination of Spent Fuel Shipment Risk Estimates*, NUREG/CR-6672, Vol. 1 (SAND2000-0234). Sandia National Laboratories, Albuquerque, New Mexico.

17. U.S. Nuclear Regulatory Commission. January 1997. "Standard Review Plan for Dry Cask Storage Systems." NUREG-1536, USNRC, Washington D.C.

18. Sandoval RP, RE Einziger, H Jordan, AP Malinauskas, and WJ Mings. January 1991. *Estimate of CRUD Contribution to Shipping Cask Containment Requirements,* SAND88-1358. Sandia National Laboratories, Albuquerque, New Mexico.

19. Larson DW, RT Reese, and EL Wilmot. January 1983. *The Caldecott Tunnel Fire Thermal Environments, Regulatory Considerations and Probabilities*, SAND-82-1949C;CONF-830528-8, Sandia National Laboratories, Albuquerque, New Mexico. Presented at 7th International Symposium on Packaging and Transportation of Radioactive Materials, 15 May 1983, New Orleans, LA.

Appendix A

Material Properties for ANSYS Model of Legal Weight Truck Package

Table A.1. 304 Stainless Steel

Temperature (°F)	Thermal Conductivity (Btu/hr-in-°F)	Density (lbm/in^3)	Specific Heat (Btu/lbm-°F)	Description
70	0.7143	-	0.1141	Used for cask body, cask lid, spokes
212	0.7800	0.2888	0.1207	
392	0.8592	0.2872	0.1272	
572	0.9333	0.2855	0.1320	
752	1.0042	0.2839	0.1356	
932	1.0717	0.2822	0.1385	
1112	1.1375	0.2805	0.1412	

Table A.2. 6061-T6 Aluminum

Temperature (°F)	Thermal Conductivity (Btu/hr-in-°F)	Density (lbm/in^3)	Specific Heat (Btu/lbm-°F)	Description
32	9.7500	0.0984	0.2140	Used for basket, IL 1, 2 skin
212	9.9167			
572	11.0833			
932	12.9167			

Table A.3. 6061-T6 Aluminum Honeycomb

Temperature (°F)	Thermal Conductivity (Btu/hr-in-°F)	Density (lbm/in^3)	Specific Heat (Btu/lbm-°F)	Description
32	1.6965	0.017118056	0.214	Used for IL 1 (Honeycomb)
212	1.7255			
572	1.9285			
932	2.2475			

Table A.4. 6061-T6 Aluminum Honeycomb

Temperature (°F)	Thermal Conductivity (Btu/hr-in-°F)	Density (lbm/in^3)	Specific Heat (Btu/lbm-°F)	Description
32	1.4235	0.0144	0.214	Used for IL 2 (Honeycomb)
212	1.4478			
572	1.6182			
932	1.8858			

Table A.5. Helium

Temperature (°F)	Thermal Conductivity (Btu/hr-in-°F)	Density (lbm/in^3)	Specific Heat (Btu/lbm-°F)	Description
200	0.00808	4.83E-06	1.24	Used for cask gap and fuel gap
400	0.00942	3.70E-06		
600	0.01075	3.01E-06		
800	0.0115	2.52E-06		

Table A.6. Chemical Copper Lead

Temperature (°F)	Thermal Conductivity (Btu/hr-in-°F)	Density (lbm/in^3)	Specific Heat (Btu/lbm-°F)	Description
68	1.6651	0.3	0.06	Used for lead regions
209	1.6308			
400	1.526			
499	1.4111			
581	1.2096			
630	1.0079			

Table A.7. 56% Ethylene Glycol Solution

Avg. Temperature (°F)	Thermal Conductivity (Btu/hr-in-°F)	Specific Heat (Btu/lbm-°F)	Density (lbm/in^3)
50	0.0188	0.7405	0.0391
70	0.0187	0.7522	0.0389
100	0.0185	0.7696	0.0385
150	0.0182	0.7979	0.0378
200	0.0179	0.8255	0.0370
250	0.0177	0.8522	0.0362
260	0.0176	0.8575	0.0360
270	0.0176	0.8627	0.0358
280	0.0175	0.8679	0.0357
290	0.0175	0.8731	0.0355
300	0.0174	0.8782	0.0353
310	0.0174	0.8833	0.0351
320	0.0173	0.8884	0.0349
330	0.0173	0.8934	0.0347
340	0.0172	0.8984	0.0345
350	0.0172	0.9034	0.0343

Table A.8. Air

Avg. Temperature (°F)	Thermal Conductivity (Btu/hr-in-°F)	Specific Heat (Btu/lbm-°F)	Density (lbm/in^3)
350	0.0017	0.2467	0.0000283
450	0.0018	0.2494	0.0000252
550	0.0020	0.2516	0.0000227
650	0.0022	0.2533	0.0000206
750	0.0023	0.2546	0.0000189
850	0.0025	0.2556	0.0000175
950	0.0026	0.2562	0.0000162
1050	0.0027	0.2566	0.0000152
1150	0.0029	0.2568	0.0000142
1250	0.0030	0.2570	0.0000134
1350	0.0031	0.2571	0.0000126
1450	0.0033	0.2571	0.0000120
1550	0.0034	0.2573	0.0000114
1650	0.0035	0.2576	0.0000108
1750	0.0036	0.2581	0.0000104
1850	0.0038	0.2589	0.0000099
1950	0.0039	0.2599	0.0000095
2050	0.0040	0.2614	0.0000091

Table A.9. Effective Conductivity for Liquid Neutron Shield with 1°F Temperature Gradient

Avg. Temperature (°F)	56% Ethylene Glycol		Air	
	Effective Conductivity Neutron Shield (Btu/hr-in-°F)	Effective Conductivity Expansion Tank (Btu/hr-in-°F)	Effective Conductivity Neutron Shield (Btu/hr-in-°F)	Effective Conductivity Expansion Tank (Btu/hr-in-°F)
250	0.364	0.149	0.003	0.002
260	0.374	0.153	0.003	0.002
270	0.384	0.157	0.003	0.002
280	0.393	0.161	0.003	0.002
290	0.398	0.163	0.003	0.002
300	0.396	0.162	0.003	0.002
310	0.395	0.162	0.003	0.002
320	0.394	0.161	0.003	0.002
330	0.393	0.161	0.003	0.002
340	0.391	0.160	0.003	0.002
350	0.390	0.160	0.003	0.002
351	*	*	0.003	0.002
400	*	*	0.003	0.002
500	*	*	0.003	0.002
600	*	*	0.003	0.002
700	*	*	0.003	0.002
800	*	*	0.003	0.002
1000	*	*	0.003	0.003
1200	*	*	0.003	0.003
1500	*	*	0.003	0.003
2000	*	*	0.004	0.004
2500	*	*	0.004	0.004

Table A.10. Effective Conductivity for Liquid Neutron Shield with 10°F Temperature Gradient

Avg. Temperature (°F)	56% Ethylene Glycol		Air	
	Effective Conductivity Neutron Shield (Btu/hr-in-°F)	Effective Conductivity Expansion Tank (Btu/hr-in-°F)	Effective Conductivity Neutron Shield (Btu/hr-in-°F)	Effective Conductivity Expansion Tank (Btu/hr-in-°F)
250	0.654	0.268	0.006	0.002
260	0.673	0.276	0.006	0.002
270	0.691	0.283	0.006	0.002
280	0.704	0.288	0.006	0.002
290	0.705	0.289	0.006	0.002
300	0.703	0.288	0.006	0.002
310	0.701	0.287	0.006	0.002
320	0.699	0.286	0.006	0.002
330	0.697	0.286	0.006	0.002
340	0.695	0.285	0.006	0.002
350	*	*	0.006	0.002
351	*	*	0.006	0.002
400	*	*	0.006	0.002
500	*	*	0.006	0.002
600	*	*	0.005	0.002
700	*	*	0.005	0.002
800	*	*	0.005	0.002
1000	*	*	0.005	0.003
1200	*	*	0.005	0.003
1500	*	*	0.004	0.003
2000	*	*	0.004	0.004
2500	*	*	0.004	0.004

Table A.11. Effective Conductivity for Liquid Neutron Shield with 25°F Temperature Gradient

Avg. Temperature (°F)	56% Ethylene Glycol		Air	
	Effective Conductivity Neutron Shield (Btu/hr-in-°F)	Effective Conductivity Expansion Tank (Btu/hr-in-°F)	Effective Conductivity Neutron Shield (Btu/hr-in-°F)	Effective Conductivity Expansion Tank (Btu/hr-in-°F)
250	0.840	0.344	0.008	0.003
260	0.863	0.353	0.008	0.003
270	0.882	0.361	0.008	0.003
280	0.888	0.364	0.008	0.003
290	0.885	0.363	0.007	0.003
300	0.883	0.361	0.007	0.003
310	0.880	0.360	0.007	0.003
320	0.877	0.359	0.007	0.003
330	0.875	0.358	0.007	0.003
340	0.872	0.357	0.007	0.003
350	*	*	0.007	0.003
351	*	*	0.007	0.003
400	*	*	0.007	0.003
500	*	*	0.007	0.003
600	*	*	0.007	0.003
700	*	*	0.007	0.003
800	*	*	0.006	0.003
1000	*	*	0.006	0.003
1200	*	*	0.006	0.003
1500	*	*	0.005	0.003
2000	*	*	0.005	0.004
2500	*	*	0.005	0.004

Table A.12. Effective Conductivity for Liquid Neutron Shield with 50°F Temperature Gradient

Avg. Temperature (°F)	56% Ethylene Glycol		Air	
	Effective Conductivity Neutron Shield (Btu/hr-in-°F)	Effective Conductivity Expansion Tank (Btu/hr-in-°F)	Effective Conductivity Neutron Shield (Btu/hr-in-°F)	Effective Conductivity Expansion Tank (Btu/hr-in-°F)
250	1.061	0.434	0.009	0.004
260	1.058	0.433	0.009	0.004
270	1.055	0.432	0.009	0.004
280	1.052	0.431	0.009	0.004
290	1.049	0.430	0.009	0.004
300	1.046	0.428	0.009	0.004
310	1.043	0.427	0.009	0.004
320	1.039	0.426	0.009	0.004
330	*	*	0.009	0.004
340	*	*	0.009	0.004
350	*	*	0.009	0.004
351	*	*	0.009	0.004
400	*	*	0.009	0.003
500	*	*	0.008	0.003
600	*	*	0.008	0.003
700	*	*	0.008	0.003
800	*	*	0.008	0.003
1000	*	*	0.007	0.003
1200	*	*	0.007	0.003
1500	*	*	0.006	0.003
2000	*	*	0.006	0.004
2500	*	*	0.006	0.004

Table A.13. Effective Conductivity for Liquid Neutron Shield with 70°F Temperature Gradient

Avg. Temperature (°F)	56% Ethylene Glycol		Air	
	Effective Conductivity Neutron Shield (Btu/hr-in-°F)	Effective Conductivity Expansion Tank (Btu/hr-in-°F)	Effective Conductivity Neutron Shield (Btu/hr-in-°F)	Effective Conductivity Expansion Tank (Btu/hr-in-°F)
250	1.151	0.471	0.010	0.004
260	1.148	0.470	0.010	0.004
270	1.144	0.469	0.010	0.004
280	1.141	0.467	0.010	0.004
290	1.138	0.466	0.010	0.004
300	1.134	0.464	0.010	0.004
310	1.131	0.463	0.010	0.004
320	*	*	0.010	0.004
330	*	*	0.010	0.004
340	*	*	0.009	0.004
350	*	*	0.009	0.004
351	*	*	0.009	0.004
400	*	*	0.009	0.004
500	*	*	0.009	0.004
600	*	*	0.009	0.004
700	*	*	0.008	0.003
800	*	*	0.008	0.003
1000	*	*	0.008	0.003
1200	*	*	0.007	0.003
1500	*	*	0.007	0.003
2000	*	*	0.006	0.004
2500	*	*	0.006	0.004

Table A.14. Effective Conductivity for Liquid Neutron Shield with 100°F Temperature Gradient

Avg. Temperature (°F)	56% Ethylene Glycol		Air	
	Effective Conductivity Neutron Shield (Btu/hr-in-°F)	Effective Conductivity Expansion Tank (Btu/hr-in-°F)	Effective Conductivity Neutron Shield (Btu/hr-in-°F)	Effective Conductivity Expansion Tank (Btu/hr-in-°F)
250	1.253	0.513	0.011	0.004
260	1.249	0.512	0.011	0.004
270	1.245	0.510	0.011	0.004
280	1.242	0.509	0.011	0.004
290	1.238	0.507	0.011	0.004
300	1.234	0.505	0.011	0.004
310	*	*	0.010	0.004
320	*	*	0.010	0.004
330	*	*	0.010	0.004
340	*	*	0.010	0.004
350	*	*	0.010	0.004
351	*	*	0.010	0.004
400	*	*	0.010	0.004
500	*	*	0.010	0.004
600	*	*	0.009	0.004
700	*	*	0.009	0.004
800	*	*	0.009	0.004
1000	*	*	0.008	0.003
1200	*	*	0.008	0.003
1500	*	*	0.008	0.003
2000	*	*	0.007	0.004
2500	*	*	0.007	0.004

Table A.15. Effective Conductivity for Liquid Neutron Shield with 200°F Temperature Gradient

Avg. Temperature (°F)	56% Ethylene Glycol		Air	
	Effective Conductivity Neutron Shield (Btu/hr-in-°F)	Effective Conductivity Expansion Tank (Btu/hr-in-°F)	Effective Conductivity Neutron Shield (Btu/hr-in-°F)	Effective Conductivity Expansion Tank (Btu/hr-in-°F)
250	1.468	0.601	0.013	0.005
260	*	*	0.013	0.005
270	*	*	0.013	0.005
280	*	*	0.013	0.005
290	*	*	0.013	0.005
300	*	*	0.012	0.005
310	*	*	0.012	0.005
320	*	*	0.012	0.005
330	*	*	0.012	0.005
340	*	*	0.012	0.005
350	*	*	0.012	0.005
351	*	*	0.012	0.005
400	*	*	0.012	0.005
500	*	*	0.012	0.005
600	*	*	0.011	0.004
700	*	*	0.011	0.004
800	*	*	0.011	0.004
1000	*	*	0.010	0.004
1200	*	*	0.010	0.004
1500	*	*	0.009	0.004
2000	*	*	0.008	0.004
2500	*	*	0.008	0.005

Table A.16. Effective Conductivity for Liquid Neutron Shield with 300°F Temperature Gradient

Avg. Temperature (°F)	56% Ethylene Glycol		Air	
	Effective Conductivity Neutron Shield (Btu/hr-in-°F)	Effective Conductivity Expansion Tank (Btu/hr-in-°F)	Effective Conductivity Neutron Shield (Btu/hr-in-°F)	Effective Conductivity Expansion Tank (Btu/hr-in-°F)
250	*	*	0.014	0.005
260	*	*	0.014	0.005
270	*	*	0.014	0.005
280	*	*	0.014	0.005
290	*	*	0.014	0.005
300	*	*	0.014	0.005
310	*	*	0.014	0.005
320	*	*	0.014	0.005
330	*	*	0.014	0.005
340	*	*	0.014	0.005
350	*	*	0.013	0.005
351	*	*	0.013	0.005
400	*	*	0.013	0.005
500	*	*	0.013	0.005
600	*	*	0.012	0.005
700	*	*	0.012	0.005
800	*	*	0.012	0.005
1000	*	*	0.011	0.004
1200	*	*	0.011	0.004
1500	*	*	0.010	0.004
2000	*	*	0.009	0.004
2500	*	*	0.009	0.005

Table A.17. Effective Conductivity for Liquid Neutron Shield with 500°F Temperature Gradient

Avg. Temperature (°F)	56% Ethylene Glycol		Air	
	Effective Conductivity Neutron Shield (Btu/hr-in-°F)	Effective Conductivity Expansion Tank (Btu/hr-in-°F)	Effective Conductivity Neutron Shield (Btu/hr-in-°F)	Effective Conductivity Expansion Tank (Btu/hr-in-°F)
250	*	*	0.016	0.006
260	*	*	0.016	0.006
270	*	*	0.016	0.006
280	*	*	0.016	0.006
290	*	*	0.016	0.006
300	*	*	0.015	0.006
310	*	*	0.015	0.006
320	*	*	0.015	0.006
330	*	*	0.015	0.006
340	*	*	0.015	0.006
350	*	*	0.015	0.006
351	*	*	0.015	0.006
400	*	*	0.015	0.006
500	*	*	0.014	0.006
600	*	*	0.014	0.005
700	*	*	0.014	0.005
800	*	*	0.013	0.005
1000	*	*	0.013	0.005
1200	*	*	0.012	0.005
1500	*	*	0.011	0.005
2000	*	*	0.011	0.004
2500	*	*	0.010	0.005

Table A.18. Emissivity Values for Radiation Heat Transfer

Component	Material	Emissivity Before Fire	Emissivity During/After Fire
Canister	stainless steel	0.36	0.36
Cask	stainless steel	0.36	0.36
Outer Neutron Shield		0.34	0.34
Inner Neutron Shield		0.34	0.34
Basket	stainless steel	0.36	0.36
Fuel Clad	zircaloy	0.8	0.8
Boral Plate	aluminum clad	0.55	0.55
Shell Interior	stainless steel	0.36	0.36
Cask Exterior	stainless steel	0.85	0.9
Tunnel/ISO	various		0.9

NRC FORM 335 (9-2004) NRCMD 3.7

U.S. NUCLEAR REGULATORY COMMISSION

BIBLIOGRAPHIC DATA SHEET

(See instructions on the reverse)

1. REPORT NUMBER (Assigned by NRC, Add Vol., Supp., Rev., and Addendum Numbers, if any.)

NUREG/CR-6894

2. TITLE AND SUBTITLE

Spent Fuel Transportation Package Response to the Caldecott Tunnel Fire Scenario

Draft report for comment

3. DATE REPORT PUBLISHED

MONTH	YEAR
February	2006

4. FIN OR GRANT NUMBER

J5167

5. AUTHOR(S)

H. E. Adkins, Jr.
B. J. Koeppel
J. M. Cuta

6. TYPE OF REPORT

Technical

7. PERIOD COVERED *(Inclusive Dates)*

8. PERFORMING ORGANIZATION - NAME AND ADDRESS *(If NRC, provide Division, Office or Region, U.S. Nuclear Regulatory Commission, and mailing address; if contractor, provide name and mailing address.)*

Pacific Northwest National Laboratory
Richland, WA 99352

9. SPONSORING ORGANIZATION - NAME AND ADDRESS *(If NRC, type "Same as above"; if contractor, provide NRC Division, Office or Region, U.S. Nuclear Regulatory Commission, and mailing address.)*

Spent Fuel Project Office
Office of Nuclear Material Safety and Safeguards
U.S. Nuclear Regulatory Commission
Washington, D.C. 20555-0001

10. SUPPLEMENTARY NOTES

11. ABSTRACT *(200 words or less)*

On April 7, 1982, a tank truck and trailer carrying 8,800 gallons of gasoline was involved in an accident in the Caldecott tunnel on State Route 24 near Oakland, California. The tank trailer overturned and subsequently caught fire. The U.S. Nuclear Regulatory Commission selected this accident for analysis to determine the possible regulatory implications. The staff concluded that small transportation casks similar to the NAC LWT cask would probably experience degradation of some seals in this severe accident scenario. However, any release is expected to be very small.

USNRC staff evaluated the radiological consequences of the package response to the Caldecott tunnel fire. The results of this evaluation strongly indicate that neither spent nuclear fuel (SNF) particles nor fission products would be released from a spent fuel shipping cask involved in a severe tunnel fire such as the Caldecott Tunnel Fire. The NAC LWT cask design analyzed for the Caldecott Tunnel fire scenario does not reach internal temperatures that could result in rupture of the fuel cladding. Therefore, radioactive material (i.e., SNF particles or fission products) would be retained within the fuel rods. The potential release calculated for the NAC LWT cask in this scenario indicates that any release of CRUD from the cask would be very small.

12. KEY WORDS/DESCRIPTORS *(List words or phrases that will assist researchers in locating the report.)*

Spent fuel transportation
Cask thermal performance
Thermal analysis

13. AVAILABILITY STATEMENT

unlimited

14. SECURITY CLASSIFICATION

(This Page) unclassified

(This Report) unclassified

15. NUMBER OF PAGES

16. PRICE

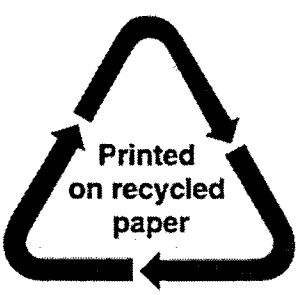

Federal Recycling Program